Rutin ameliorates obesity through brown fat activation

Article *in* The FASEB Journal · October 2016

DOI: 10.1096/fj.201600459RR

The FASEB Journal article fj.201600459RR. Published online October 20, 2016.

Rutin ameliorates obesity through brown fat activation

Xiaoxue Yuan,[*,†,1] Gang Wei,[*,†,1] Yilin You,[‡,1] Yuanyuan Huang,[*,†] Hyuek Jong Lee,[*] Meng Dong,[*,†] Jun Lin,[*,†] Tao Hu,[*,†] Hanlin Zhang,[*] Chuanhai Zhang,[*] Huiqiao Zhou,[*,†] Rongcai Ye,[*,†] Xiaolong Qi,[†,§] Baiqiang Zhai,[‡] Weidong Huang,[‡] Shunai Liu,[¶] Wen Xie,[¶] Qingsong Liu,[‖] Xiaomeng Liu,[#] Chengbi Cui,[**] Donghao Li,[**] Jicheng Zhan,[‡,2] Jun Cheng,[¶,2] Zengqiang Yuan,[†,§,2,3] and Wanzhu Jin[*,2,4]

[*]Key Laboratory of Animal Ecology and Conservation Biology, Institute of Zoology, and [§]State Key Laboratory of Brain and Cognitive Sciences, Institute of Biophysics, Chinese Academy of Sciences, Beijing, China; [†]The University of the Chinese Academy of Sciences, Beijing, China; [‡]Beijing Advanced Innovation Center for Food Nutrition and Human Health, College of Food Science and Nutritional Engineering, China Agricultural University, Beijing, China; [¶]Institute of Infectious Diseases, Beijing Ditan Hospital, Capital Medical University, Beijing, China; [‖]High Magnetic Field Laboratory, Chinese Academy of Sciences, Hefei, China; [#]College of Life Sciences, Zhoukou Normal University, Henan, China; and [**]Key Laboratory of Natural Resources of Changbai Mountain and Functional Molecules, Ministry of Education, Yanbian University, Yanji, China

ABSTRACT: Increasing energy expenditure through activation of brown adipose tissue (BAT) is a critical approach to treating obesity and diabetes. In this study, rutin, a natural compound extracted from mulberry and a drug used as a capillary stabilizer clinically for many years without any side effects, regulated whole-body energy metabolism by enhancing BAT activity. Rutin treatment significantly reduced adiposity, increased energy expenditure, and improved glucose homeostasis in both genetically obese (Db/Db) and diet-induced obesity (DIO) mice. Rutin also induced brown-like adipocyte (beige) formation in subcutaneous adipose tissue in both obesity mouse models. Mechanistically, we found that rutin directly bound to and stabilized SIRT1, leading to hypoacetylation of peroxisome proliferator-activated receptor γ coactivator-1α protein, which stimulated Tfam transactivation and eventually augmented the number of mitochondria and UCP1 activity in BAT. These findings reveal that rutin is a novel small molecule that activates BAT and may provide a novel therapeutic approach to the treatment of metabolic disorders.—Yuan, X., Wei, G., You, Y., Huang, Y., Lee, H. J., Dong, M., Lin, J., Hu, T., Zhang, H., Zhang, C., Zhou, H., Ye, R., Qi, X., Zhai, B., Huang, W., Liu, S., Xie, W., Liu, Q., Liu, X., Cui, C., Li, D., Zhan, J., Cheng, J., Yuan, Z., Jin, W. Rutin ameliorates obesity through brown fat activation. FASEB J. 31, 000–000 (2017). www.fasebj.org

KEY WORDS: brown adipose tissue · rutin · obesity · energy expenditure · mitochondria

The incidence of obesity has dramatically increased over the past few decades and has become a global health problem worldwide. Obesity is a result of excess body fat accumulation, which often causes adverse effects on human health, such as cardiovascular disease, type 2 diabetes mellitus, hypertension, cancer, and other related diseases (1). Obesity develops when energy intake exceeds energy expenditure and the excess energy is stored in white adipose tissue (WAT) as a form of triglyceride (2). Current antiobesity strategies are aimed at restricting energy uptake and absorption; however, obesity is far from being dealt with satisfactorily. Therefore, an effective alternative strategy is urgently needed to increase energy expenditure in key metabolic organs such as brown adipose tissue (BAT) (3).

Mammalian fat tissues are mainly divided into 2 types of fat tissues with opposing functions: BAT and WAT (4). BAT, histologically distinct from WAT, is composed of multilocular lipid droplets and a large number of mitochondria that generate heat to maintain body temperature through a process called nonshivering thermogenesis (5). Previous studies have shown that BAT potentially protects against obesity and its related diseases, which opens a novel avenue to combating obesity (6–8). BAT was initially thought to facilitate adaptation to cold environments in rodents and in newborn infants. Recent studies have revealed that adult humans also have functional BAT

ABBREVIATIONS: BAT, brown adipose tissue; DIO, diet-induced obesity; FDG, fluorodeoxyglucose; GTT, glucose tolerance test; HEK, human embryonic kidney; HEPES, 4-(2-hydroxyethyl)-1-piperazineethanesulfonic acid; HFD, high-fat diet; ITC, isothermal titration calorimetry; KO, knockout; mtDNA, mitochondrial DNA; NRF, nuclear respiratory factor; oxphos, oxidative phosphorylation; PGC, peroxisome proliferator-activated receptor γ coactivator; qPCR, quantitative PCR; RER, respiratory exchange ratio; ROI, region of interest; SIRT1, NAD-dependent deacetylase sirtuin-1; STAC, SIRT1-activating compound; sWAT, subcutaneous white adipose tissue; Tfam, mitochondrial transcription factor A; TSA, trichostatin A; UCP1, uncoupling protein 1; WAT, white adipose tissue; WT, wild-type

[1] These authors contributed equally to this work.
[2] These authors contributed equally to this work.
[3] Correspondence: State Key Laboratory of Brain and Cognitive Sciences, Institute of Biophysics, Chinese Academy of Sciences, Beijing, 100101, China. E-mail: zqyuan@ibp.ac.cn
[4] Correspondence: Key Laboratory of Animal Ecology and Conservation Biology Institute of Zoology, Chinese Academy of Sciences, Beijing, 100101, China. E-mail: jinw@ioz.ac.cn;

doi: 10.1096/fj.201600459RR
This article includes supplemental data. Please visit *http://www.fasebj.org* to obtain this information.

(9–11) and various stimuli could recruit uncoupling protein (UCP)-1-positive multilocular adipocytes in WAT, which is defined as beige or brite (brown in white) (12). Recently, irisin and PRDM16 have been found to stimulate beige formation in WAT, resulting in the augmentation of energy expenditure (13, 14). Therefore, increasing BAT activity and induction of beige formation could be a novel and effective therapeutic approach to the prevention and cure of obesity and its related diseases.

In our recent study, we showed that mulberry extract increases the number of mitochondria and expression of BAT-specific thermogenic genes during *in vitro* brown adipogenesis (15). Furthermore, we found that mulberry extract contains a large amount of anthocyanin, such as cyanidin 3-glucoside (C3G) and rutin. Rutin is an important flavonoid that is consumed in the daily diet. *In vivo* and *in vitro* studies have shown that it can exhibit significant pharmacological activities, including antioxidation and anti-inflammation, and antidiabetic properties (16–18). Although rutin has been demonstrated to block high-fat-diet-induced obesity and to have beneficial effects on blood lipids and glucose levels in recent years (18), the underlying molecular mechanisms are largely unknown. For the first time, we demonstrated that rutin increases energy expenditure by activating BAT and inducing beige tissue formation in genetic obese Db/Db (leptin receptor-deficient) and DIO mouse models. In addition, rutin functions as a cold mimetic through activating the sirtuin 1 (SIRT1)/peroxisome proliferator-activated receptor γ coactivator (PGC)-1α/mitochondrial transcription factor (Tfam) signaling cascade and increasing the number of mitochondria and UCP1 activity in BAT. Our data establish that rutin plays a previously unrecognized role in combating obesity, which may provide a novel therapeutic approach to the treatment of metabolic disorders.

MATERIALS AND METHODS

Animals

Obese C57BLKS/J-Leprdb/Leprdb (Db/Db) male mice (3-wk-old) were purchased from the Model Animal Research Center of Nanjing University. Three-week-old male C57BL/6J mice from Vital River Laboratory Animal Technology (Beijing, China) were fed either a low-fat (LFD) or high-fat (HFD) diet. The LFD (12450Bi) and HFD (D12492i) contain 10 kcal% fat and 60 kcal% fat, respectively (Research Diets, New Brunswick, NJ, USA). Rutin (1 mg/ml) was added to the drinking water of the mice for 10 wk. The mice were fed *ad libitum* and euthanized under mild ether anesthesia. All animal studies were approved by the Institutional Animal Care and Use Committee of Institute of Zoology (Chinese Academy of Sciences).

Glucose tolerance test

Mice were left unfed for 16 h (5:00 PM to9:00 AM) with free access to drinking water. Glucose (1 g/kg for Db/Db mice and 1.5 g/kg for HFD mice) was administered intraperitoneally, and blood glucose levels were measured with an Accu-Chek glucose monitor (Roche Diagnostics, Indianapolis, IN, USA) at various time points (see Results). If the blood glucose value was higher than the measuring range of the commercial glucometers, we diluted the sample in saline and repeated the measurement. Thereafter, we multiplied the result by the dilution factor as the final blood glucose value.

Metabolic rate and physical activity

Oxygen consumption and physical activity were determined at 12 wk of age with a TSE lab master, as previously described (19). Mice were acclimated to the system for 20–24 h, and then Vo_2 and Vco_2 were measured during the next 24 h. The animals were maintained at 24°C in a 12-h light/dark cycle with free access to food and water. Voluntary activity of each mouse was measured with an optical beam technique (Opto-M3, Columbus Instruments, Columbus, OH, USA) over 24 h and expressed as 24-h average activity. Heat production and respiratory exchange ratio (RER) were then calculated (20).

Body composition measurements

The total fat and lean masses of mice after a 7-wk treatment with either vehicle or rutin were assessed with the Small Animal Body Composition Analysis and Imaging System (MesoQMR 23-060H-I; Nuimag Corp., Shanghai, China), according to the manufacturer's instructions.

Cold-induced thermogenesis

A cold tolerance test was performed in 13-wk-old mice. The mice were placed in a cold chamber (4°C) for up to 4 h with free access to food and water. Body temperature was measured with a rectal probe connected to a digital thermometer (Yellow Spring Instruments, Yellow Springs, OH, USA).

Skin temperature measurement

Skin temperature surrounding BAT was recorded with an infrared camera (E60: Compact Infrared Thermal Imaging Camera; FLIR, West Malling, United Kingdom) and analyzed with a specific software package (IR Max 3.4; FLIR). Skin temperature surrounding the BAT was analyzed after averaging temperatures from 3 or 4 images in each animal.

Postitron emission-computed tomographic imaging

Positron emission-computed tomographic (PET-CT) imaging was achieved with the Siemens Inveon Dedicated PET (dPET) System and Inveon Multimodality (MM) System (CT-SPECT) (Siemens Preclinical Solutions, Knoxville, TN, USA) at the Institute of Laboratory Animal Sciences, Chinese Academy of Medical Sciences. The mice were left unfed overnight and were lightly anesthetized with isoflurane followed by a tail vein injection of fluorodeoxyglucose ([^{18}F]-FDG; 500 mCi). They were subjected to PET-CT analysis at 60 min after radiotracer injection. Inveon Acquisition Workplace (IAW) software (Siemens Preclinical Solutions) was used for the scanning process. A 10-min CT X-ray for attenuation correction was scanned with a power of 80 kV and 500 μA and an exposure time of 1100 ms before the PET scan. Ten-minute static PET scans were acquired, and images were reconstructed by an ordered-subsets expectation maximization (OSEM) 3-dimensional algorithm followed by maximization/maximum a posteriori (MAP) or FastMAP provided by IAW. The 3-dimensional regions of interest (ROIs) were drawn over the guided CT images, and the tracer uptake was

measured with the IRW software (Siemens). Individual quantification of the [^{18}F]-FDG uptake in each of the ROIs was calculated. The data for the accumulation of [^{18}F]-FDG on micro-PET images were expressed as the standard uptake values, which were determined by dividing the relevant ROI concentration by the ratio of the injected activity to the body weight.

Histology and bodipy staining

Tissues fixed with 4% paraformaldehyde were sectioned after being embedded in paraffin. Multiple sections were prepared for hematoxylin-eosin staining. Cells grown on poly-L-lysine-pretreated coverslips (Sigma-Aldrich, St. Louis, MO, USA) were incubated in 5% goat serum for 1 h at room temperature after fixation with 1% formalin at room temperature for 1 h, then incubated with Bodipy (Thermo Fisher Scientific, Waltham, MA, USA) for 2 h at room temperature. All images were acquired with the BX51 system (Olympus, Tokyo, Japan).

Transmission electron microscopy

BAT sections were fixed with 2% (vol/vol) glutaraldehyde in 100 mM phosphate buffer (pH 7.2) for 12 h at 4°C. Sections were then postfixed with 1% osmium tetroxide, dehydrated in ascending gradations of ethanol, and embedded in fresh epoxy resin 618. Ultrathin sections (60–80 nm) were cut and stained with lead citrate before being examined on a CM-120 transmission electron microscope (Philips, Eindhoven, The Netherlands).

Brown adipocyte differentiation

$C_3H_{10}T_{1/2}$ cells, a mouse mesenchymal stem cell line, were purchased from National Platform of Experimental Cell Resources (Sci-Tech, Shanghai, China). The cells were treated with a brown adipogenic induction cocktail [DMEM containing 10% fetal bovine serum, 20 nM insulin, 1 μM dexamethasone, 0.5 mM isobutylmethylxanthine, 125 nM indomethacin, and 1 nM 3,3,5-triiodo-L-thyronine (T3)] for the first 2 d. The medium was then replaced by that supplemented with only insulin and T3 every other day. The cells were treated with or without rutin (10 μM) for 6 d during brown adipogenesis. At d 6, fully differentiated adipocytes were used for all experiments in the study.

Measurements of cellular respiration

$C_3H_{10}T_{1/2}$ cells were treated with or without rutin (10 μM) for 6 d during brown adipogenesis. O_2 consumption of fully differentiated adipocytes was measured at d 6 with an XF24-3 extracellular flux analyzer (Agilent Technologies, Santa Clara, CA, USA). Basal respiration was also assessed in untreated cells.

Measurements of lipolysis *in vitro*

Lipolysis activity was measured as described elsewhere (21). In brief, fully differentiated brown adipocytes were treated with serum-free DMEM, with or without rutin (10 μM) for 3 h, and the medium was collected for lipolysis measurement. Extracellular glycerol release was extracted and measured as an index of lipolysis by colorimetric assay (EnzyChrom Adipolysis Assay Kit, BioAssay Systems, Hayward, CA, USA), according to the manufacturer's instructions.

Luciferase reporter assay

The mouse Tfam promoter was amplified and inserted into the *Kpn*I and *Xho*I sites (−134 to +28) of pGL3-basic (Promega, Madison, WI, USA). The $C_3H_{10}T_{1/2}$ cells were cultured in 24-well plates and cotransfected with PGC1α plasmid (0.4 mg/well), NRF2 plasmid (0.4 mg/well), and luciferase reporter construct (0.4 mg/well) with the Profection kit (Promega), according to the manufacturer's protocol. The mass of transfected plasmids was balanced with empty vector (pCDH-EGFP). After 48 h, the cells were harvested, and luciferase activity was measured with the Dual-Luciferase Reporter assay system (Promega). Renilla luciferase activity was used to normalize for transfection efficiency.

NRF2 and PGC1α binding assay

Human embryonic kidney (HEK)293T cells were transfected with NRF2 and PGC1α, alone and in combination. Cell lysates were collected in RIPA buffer 48 h after transfection. NRF2 protein was immunoprecipitated with anti-NRF2 antibody (sc-28696; Santa Cruz Biotechnology, Santa Cruz, CA, USA). NRF2 was Western blotted with anti-NRF2 antibody (sc-6059; Santa Cruz Biotechnology) and anti-PGC1α antibody (AB3242; EMS–Millipore, Billerica, MA, USA).

PGC1α acetylation assay

$C_3H_{10}T_{1/2}$ cells were transfected with His-PGC1α (2 μg), SIRT1 (0.5 μg), and p300 (0.5 μg). Twenty-four hours after transfection, the cells were incubated with or without rutin, and then the cell lysates were collected with IP buffer [50 mM 4-(2-hydroxyethyl)-1-piperazineethanesulfonic acid (HEPES; pH 7.9), 150 mM NaCl, 10% glycerol, 1 mM EGTA, 1% Triton X-100, 0.5% NP-40, 1 μM trichostatin A (TSA), and protease inhibitor cocktail (Roche)], followed by incubation with anti-PGC1α antibody (H300; Santa Cruz Biotechnology) overnight at 4°C. Immunoprecipitates were blotted with anti-SIRT1 (Cell Signaling Technology, Danvers, MA, USA), anti-PGC1α (Abcam, Cambridge, United Kingdom), and anti-acetyl-lysine (EMS–Millipore) antibodies.

RNA isolation and real-time quantitative PCR

Total RNAs from tissues or cells were extracted with Trizol reagent (Thermo Fisher Scientific). Reverse transcription of total RNA (2 μg) was performed with a high-capacity cDNA reverse transcription kit (Promega). Real-time quantitative PCR (qPCR) was performed with a SYBR Green Master Mix (Promega). The PCR reaction was run in triplicate for each sample using a Prism VIIA7 real-time PCR system (Thermo Fisher Scientific). See Supplemental Table S2 for the details of primer sequences.

Western blot analysis

An equal amount of protein from cell lysate was loaded into each well of a 12% SDS-polyacrylamide gel after denaturation with SDS loading buffer. After electrophoresis, proteins were transferred to a PVDF membrane, incubated with blocking buffer (5% fat-free milk) for 1 h at room temperature, and blotted with the following antibodies overnight: anti-UCP1, anti-oxphos, anti-Tfam, anti-PGC1α (Abcam), anti-SIRT1, anti-GAPDH (Cell Signaling Technology), and anti-β actin (Sigma-Aldrich). The membrane was incubated with horseradish peroxidase–conjugated secondary antibodies for 1 h at room temperature. All signals were visualized and analyzed by densitometric scanning (Image Quant TL7.0; GE Healthcare Biosciences, Uppsala Sweden). Intensity values of the

bands were quantified by using ImageJ software (National Institutes of Health, Bethesda, MD, USA).

Measurement of mitochondrial copy number

Total DNAs [genomic and mitochondrial DNA (mtDNA)] were isolated from $C_3H_{10}T_{1/2}$ cells, BAT and subcutaneous (s)WAT with the QiaAmp DNA Mini kit (Qiagen, Hilden, Germany) according to the manufacturer's instructions. DNA concentration was assessed with a Nanodrop 2000 (Thermo Fisher Scientific). mtDNA copy number relative to genomic DNA content was quantitatively analyzed with a Prism VIIA7 real-time PCR system (Thermo Fisher Scientific). Primer sequences for COX II and β-globin were as follows: COX II: (forward) GCCGACTAAATCAAGCAACA, (reverse) CAATGGGCATAAAGCTATGG; and β globin: (forward) GAAGCGATTCTAGGGAGCAG, (reverse) GGAGCAGCGATTCTGAGTAG.

Isothermal titration calorimetric measurements

Isothermal titration calorimetric (ITC) measurement were performed with an ITC200 calorimeter (MicroCal LLC; Malvern Instruments, Malvern, United Kingdom) at 25°C in reaction buffer [20 mM HEPES-NaOH (pH 7.5), 150 mM NaCl, 10% glycerol, and 1.2% DMSO]. SIRT1-143 CS and mutant E230K proteins (generous gifts from Dr. Ruiming Xu, Chinese Academy of Sciences) were purified and dialyzed against the buffer, centrifuged, and thoroughly degassed before the experiment. A total of 20 aliquots of 1.5 mM peptide, with a 0.5 μl first drop (data not used) and 2 μl subsequent drops was injected from a rotating syringe (600 rpm) into a 200 μl calorimetric cell containing 0.1 mM protein solution. The initial delay was set at 60 s, and the reference power was set at 5 μcal/s. Injections were performed at 0.5 μl/s with an interval of 120 s between injections. The titrant and protein cell solution were in the same buffer [20 mM HEPES-NaOH (pH 7.5), 150 mM NaCl, 10% glycerol, and 1.2% DMSO], with or without rutin (0.5 mM). The corresponding buffer control (without peptide in the titrant) for each experiment was performed under the same condition, and the measured background heat was subtracted from the integrated data to arrive at the actual heat of interaction. The ITC data were integrated and analyzed by Origin software (Origin Lab, Northampton, MA, USA), supplied with the instrument according to a 1-site model.

In vitro deacetylation assay

HEK293 cells were cotransfected with plasmids encoding p300 and His-tagged PGC-1α. After 48 h, the cells were collected in PBS buffer (pH7.5) containing 330 mM NaCl, 0.5% Tween-20, 20% glycerol, 1 μM TSA, 10 mM imidazole, and protease inhibitor cocktail (Roche), and were lysed with sonication in an ultrasonic processor (Scientz-IID; Ningbo Scientz, Ningbo City, China). To capture the maximum quantity of acetylated PGC-1α, 10 mM nicotinamide, 2 μM TSA was added for the last 10 h before harvest. Acetylated PGC-1α was purified by immobilized metal affinity chromatography of protein lysate in lysis buffer (PBS at pH7.5, containing 330 mM NaCl, 0.5% Tween-20, 20% glycerol, 1 μM TSA, and 10 mM imidazole), with Ni-NTA beads (Qiagen). Beads were collected in a drip column at 4°C directed against the hexahistidine tag. Nonspecifically bound proteins were removed *via* wash buffer (PBS at pH7.5, containing 330 mM NaCl, 0.5% Tween-20, 20% glycerol, 1 μM TSA, and 30 mM imidazole) before elution (PBS at pH7.5, containing 330 mM NaCl, 0.5% Tween-20, 20% glycerol, 1 μM TSA, and 400 mM imidazole). For the deacetylation reaction *in vitro*, an equal amount of acetylated PGC1α was incubated with 1 μg recombinant WT SIRT1 or mutant SIRT1 E230K. A deacetylation assay was performed in reaction buffer [50 mM Tris (pH 8.0), 500 mM NaCl, 4 mM $MgCl_2$, 10 mM DTT, 1 mg/ml bovine serum albumin, and 100 μM NAD^+] for 3 h at 30°C in the presence of various concentrations of rutin, and 10 mM nicotinamide was used as the negative control. After incubation with recombinant SIRT1 or E230K, the level of acetylated PGC1α was determined by blotting with anti-acetyl lysine antibody (Cell Signaling Technology).

Statistics

Data are expressed as means ± SEM. Statistical significance was tested with 1-way ANOVA followed by Tukey's *post hoc* test or a paired Student's *t* test. Statistical significance was set at $P < 0.05$.

RESULTS

Rutin increases mitochondrial biogenesis and oxygen consumption

We previously showed that mulberry extracts contain large amounts of anthocyanin pigments such as Cy-3-glu and Cy-3-rut which increase mitochondrial function during *in vitro* brown adipogenesis (15). To investigate whether rutin is involved in BAT differentiation, $C_3H_{10}T_{1/2}$ cells were used to perform an *in vitro* BAT differentiation assay, with or without rutin treatment. Rutin markedly increased the expression of *UCP1*, a BAT-specific marker, in a dose-dependent manner and with maximum effect at 10 μM concentration (**Fig. 1*A***). Consistently, Rutin also increased the expression levels of other BAT-related thermogenic genes, such as *PRDM16* and *PGC1α* (Fig. 1*B*). However, it had no significant effect on lipid accumulation (Fig. 1*C*) or on the expression of adipogenic marker genes (Fig. 1*D*). The high number of mitochondria and high rates of oxygen consumption are 2 main features of BAT. We first asked whether rutin had any effect on mitochondrial biogenesis. As expected, the expression levels of key genes in mitochondrial biogenesis such as *Tfam*, nuclear respiratory factor 1 (*NRF1*), and *NRF2* were significantly increased by rutin treatment (Fig. 1*E*). We also observed that rutin dramatically augmented the mitochondrial copy number (Fig. 1*F*). On the other hand, oxygen consumption was significantly increased by rutin treatment and was further boosted by addition of carbonyl cyanide 4-(trifluoromethoxy) phenylhydrazone (FCCP), a potent mitochondrial oxidative phosphorylation uncoupler stimulator (Fig. 1*G*). Taken together, these results indicate that rutin can effectively increase the mitochondrial biogenesis and respiratory function of brown adipocytes.

Rutin augments whole-body energy metabolism and maintains glucose homeostasis

Having found that rutin increases the mitochondrial biogenesis and respiratory function of brown adipocytes, we next investigated whether it has an effect on whole-body energy metabolism. To this end, diet-induced obesity (DIO) and genetically obese (Db/Db) mice were used to assess the interventional effects of rutin on energy metabolism. A significant reduction in body weight upon rutin treatment

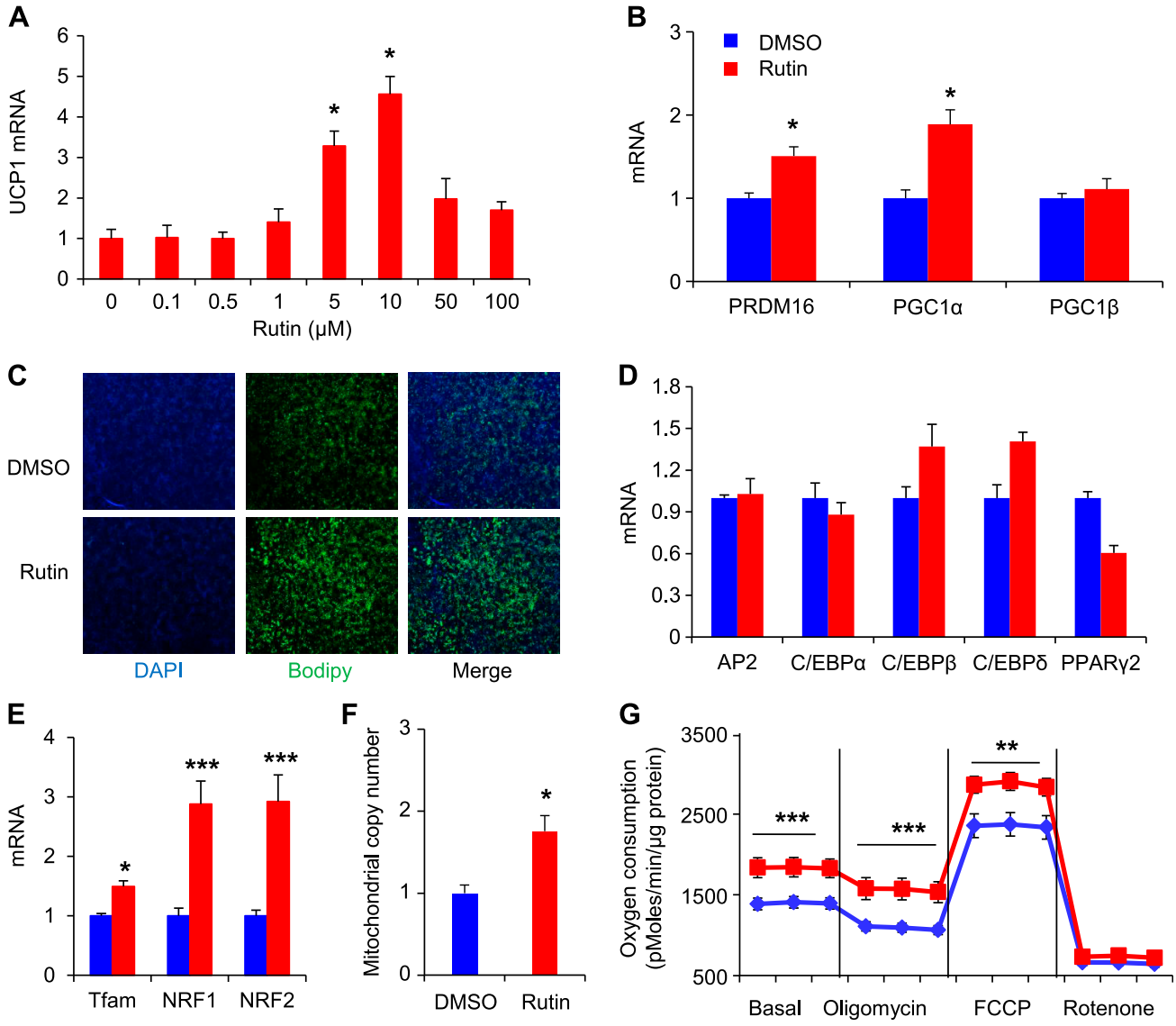

Figure 1. Rutin increases mitochondrial biogenesis and oxygen consumption. *A*) Dose-dependent effect of rutin on *UCP1* expression in $C_3H_{10}T_{1/2}$ cells at d 6 of brown adipogenesis. *B*) Thermogenic gene expression in $C_3H_{10}T_{1/2}$ cells treated with 10 μM rutin or DMSO. *C*) Representative images of Bodipy staining. $C_3H_{10}T_{1/2}$ cells were treated with 10 μM rutin or DMSO during 6 d of brown adipogenesis. *D–G*) The expression levels of adipogenic marker genes (*D*), mitochondrial biogenic genes (*E*), mitochondrial copy number (*F*), and oxygen consumption rates (OCR) (*G*) at d 6 of brown adipogenesis with 10 μM rutin or DMSO treatment. Data are means ± SEM (n = 3–6). $^*P < 0.05$, $^{**}P < 0.01$, $^{***}P < 0.001$ *vs.* control.

was observed in both mouse models (**Fig. 2*A, B*** and Supplemental Fig. S1*A*, *B*). Further studies showed that the reduction in body weight was mainly due to the improvement in adiposity (Fig. 2*C*, *D* and Supplemental Fig. S2*A*, *B*). Consistently, histologic analysis revealed that the sizes of lipid droplets in adipose tissues from rutin-treated mice were smaller than those from control mice (Supplemental Fig. S1*C–H*). In parallel, serum cholesterol and triglyceride levels were significantly reduced after rutin treatment (Supplemental Table S1). These results indicate that rutin specifically affects adipose tissue composition.

Adiposity is often accompanied by alteration of energy balance. We next examined whether rutin treatment could affect energy metabolism. Rutin significantly increased energy expenditure (Fig. 2*E–H*) without any changes in food or water intake (Supplemental Fig. S2*C*, *D*, *G*, *H*) or physical activity (Supplemental Fig. S2*E*, *I*), compared with control mice. These results strongly indicate that rutin increases energy expenditure and reduces adiposity. Furthermore, rutin treatment greatly increased core body temperature when animals were exposed to a cold environment (4°C, 4 h; Fig. 2*I–L*). In addition, the RER was decreased in Db/Db mice (Supplemental Fig. S2*F*, *J*), which indicates the flexibility of the body to switch energy sources from oxidizing glucose to fat in response to energy homeostasis.

To examine whether the decreased adiposity by rutin treatment altered glucose metabolism in our mice, we investigated glucose homeostasis by an intraperitoneal glucose tolerance test (GTT). Rutin treatment greatly improved glucose homeostasis (Fig. 2*M*, *N*). Severe hepatic steatosis has been observed in Db/Db mice (22). Histologic

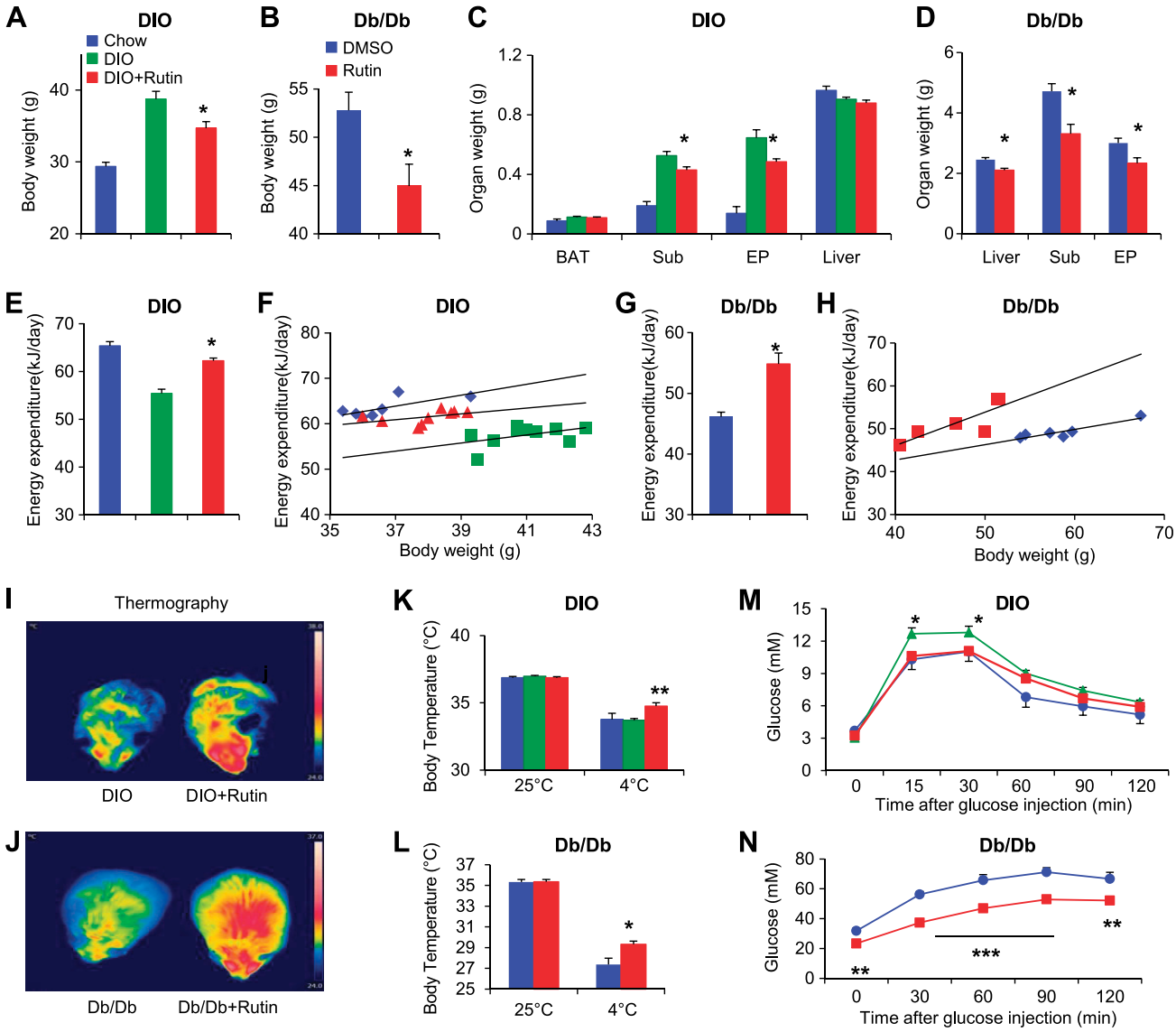

Figure 2. Rutin increases whole-body energy metabolism and glucose homeostasis. Rutin treatment significantly decreased body weight (*A*, *B*) as well as organ weight (*C*, *D*) of DIO (*A*, *C*) and Db/Db (*B*, *D*) mice. Oxygen consumption (*E–H*) and core body temperature (*I–L*) were significantly increased after rutin treatment in DIO (*E*, *F*, *I*, *K*) and Db/Db (*G*, *H*, *J*, *L*) mice. Infrared thermal images further demonstrated that rutin treatment significantly increased whole-body energy expenditure in DIO (*I*) and Db/Db (*J*) mice. In addition, results from a GTT showed that rutin significantly improved glucose homeostasis in both DIO (*M*) and Db/Db (*N*) mice. Data are means ± SEM ($n = 10$). $^*P < 0.05$, $^{**}P < 0.01$, $^{***}P < 0.0001$ *vs.* control.

examination revealed that rutin treatment ameliorated hepatic steatosis (Supplemental Fig. S3*A*, *B*). Consistently, the expression levels of inflammatory genes, such as *IL-6*, *MCP1*, and *TNFα*, in liver were dramatically decreased after rutin treatment (Supplemental Fig. S3*C*, *D*). Taken together, the evidence shows that rutin treatment greatly reduces adiposity, increases energy metabolism, maintains glucose homeostasis, and ameliorates hepatic steatosis in both Db/Db and DIO mice.

Rutin induces BAT activity

Based on the above findings, we speculated that rutin plays important roles in BAT function *in vivo*. Indeed, the expression levels of BAT markers, such as *UCP1*, *Cidea*, and *Prdm16*, were dramatically increased in BAT from rutin-treated DIO or Db/Db mice (**Fig. 3*A*, *B***). Consistently, the expression of fatty acid oxidation–related genes, including *CPT1α*, *MCAD*, *PPARα*, and *PGC1α*, was markedly increased in BAT from rutin-treated mice (Fig. 3*C*, *D*). The increased UCP1 expression in BAT from rutin-treated mice was further confirmed at the protein level (Fig. 3*E*, *F*, *L*). BAT UCP1 expression correlated closely with mitochondrial number and function. The expression of mitochondrial biogenic transcription factors, such as *Tfam*, *NRF1*, and *NRF2*, was increased more than 2-fold after rutin treatment (Fig. 3*G*, *H*). Accordingly, rutin treatment significantly raised the mitochondrial number in BAT, as evidenced by mitochondrial DNA copy number analysis (Fig. 3*I*, *J*) and electronic microscopic examination (Fig. 3*K*), but not in muscle and liver (Supplemental Fig. S4*A*, *B*).

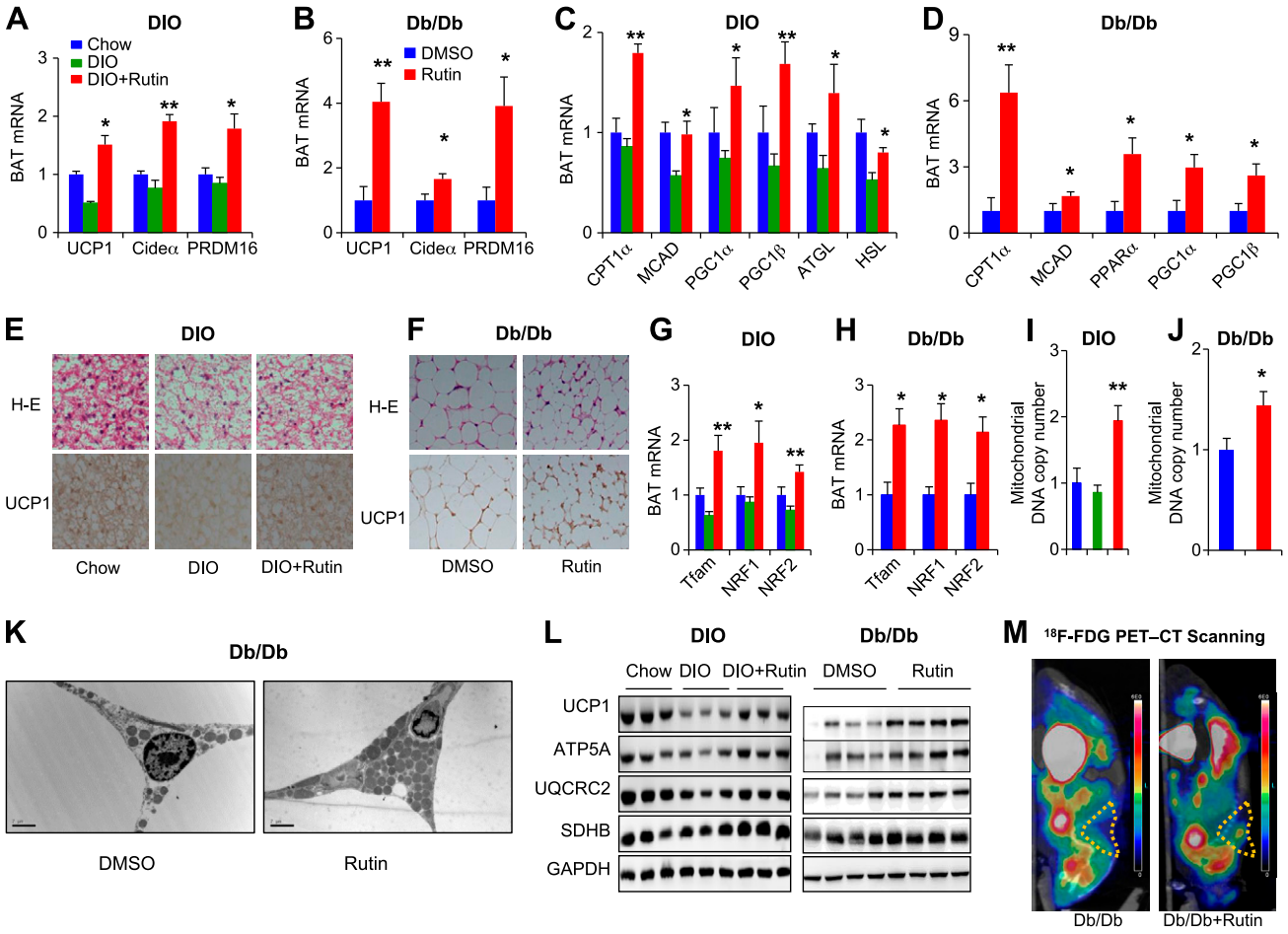

Figure 3. Rutin induces BAT activity. Rutin treatment significantly increased the expression levels of BAT thermogenic genes (*A*, *B*), fatty acid oxidation-related genes (*C*, *D*), mitochondria biogenic genes (*G*, *H*), and mitochondrial copy number (*I*, *J*) in BAT of DIO (*A*, *C*, *E*, *G*, *I*) and Db/Db (*B*, *D*, *F*, *H*, *J*–*L*) mice. Furthermore, rutin treatment significantly increased UCP1 expression (*E*, *F*, *L*) and mitochondrial oxphos protein expression in BAT of DIO and Db/Db (*L*) mice. Sagittal view of PET-CT images shows that rutin treatment significantly increased BAT activity in Db/Db mice (*M*). Yellow triangle: anatomic site of interscapular BAT. Data are means ± SEM ($n = 10$). $^*P < 0.05$, $^{**}P < 0.01$ *vs.* control.

Furthermore, the expression levels of mitochondrial oxidative phosphorylation (OXPHOS) proteins were significantly upregulated in BAT from rutin-treated mice (Fig. 3*L*). It has been reported that BAT activity is defective in Db/Db mice (23, 24). Consistently, the PET-CT analysis showed that no detectable PET signal was found in BAT from Db/Db mice, whereas rutin treatment dramatically increased the positive PET signal in BAT in Db/Db (Fig. 3*M*); the same results were observed in DIO mice (Supplemental Fig. S5*A*, *B*). These results indicate that rutin specifically and significantly increases the number of mitochondria and the BAT activity in both obesity mouse models.

Rutin induces beige cell formation in sWAT

Cold exposure induces the appearance of UCP1-positive adipocytes in WAT, which are termed "beige" cells (25). Similar to BAT, beige cells also contain a high number of mitochondria and express BAT-specific genes. Moreover, mice with increased activity of BAT or beige fat resist obesity and display improvement in systemic metabolism (6). As expected, the expression of several BAT-specific genes, including *UCP1*, *PGC1α*, *PGC1β*, *CPT1α*, and *PPARα* ,was significantly increased in sWAT after rutin treatment (**Fig. 4*C*, *D***). The expression of beige cell markers, such as *CD137* and *TBX* (12), was also significantly upregulated in sWAT from rutin-treated mice (Fig. 4*A*, *B*). Because we found that rutin treatment increased BAT mitochondrial biogenesis (Fig. 3), we then investigated the expression of *Tfam* and *NRF1/2* in rutin-treated sWAT and found that it was significantly increased after rutin treatment (Fig. 4*E*, *F*). Consistently, rutin significantly increased mitochondrial copy number and oxphos protein expression in sWAT in both mouse obesity models (Fig. 4*G*–*J*). Together, these results indicate that rutin treatment increases beige cell formation through regulating mitochondrial biogenesis.

Rutin stabilizes SIRT1 and increases deacetylase activity

Activation of PGC1α plays an important role in mitochondrial biogenesis (26). It has been demonstrated that

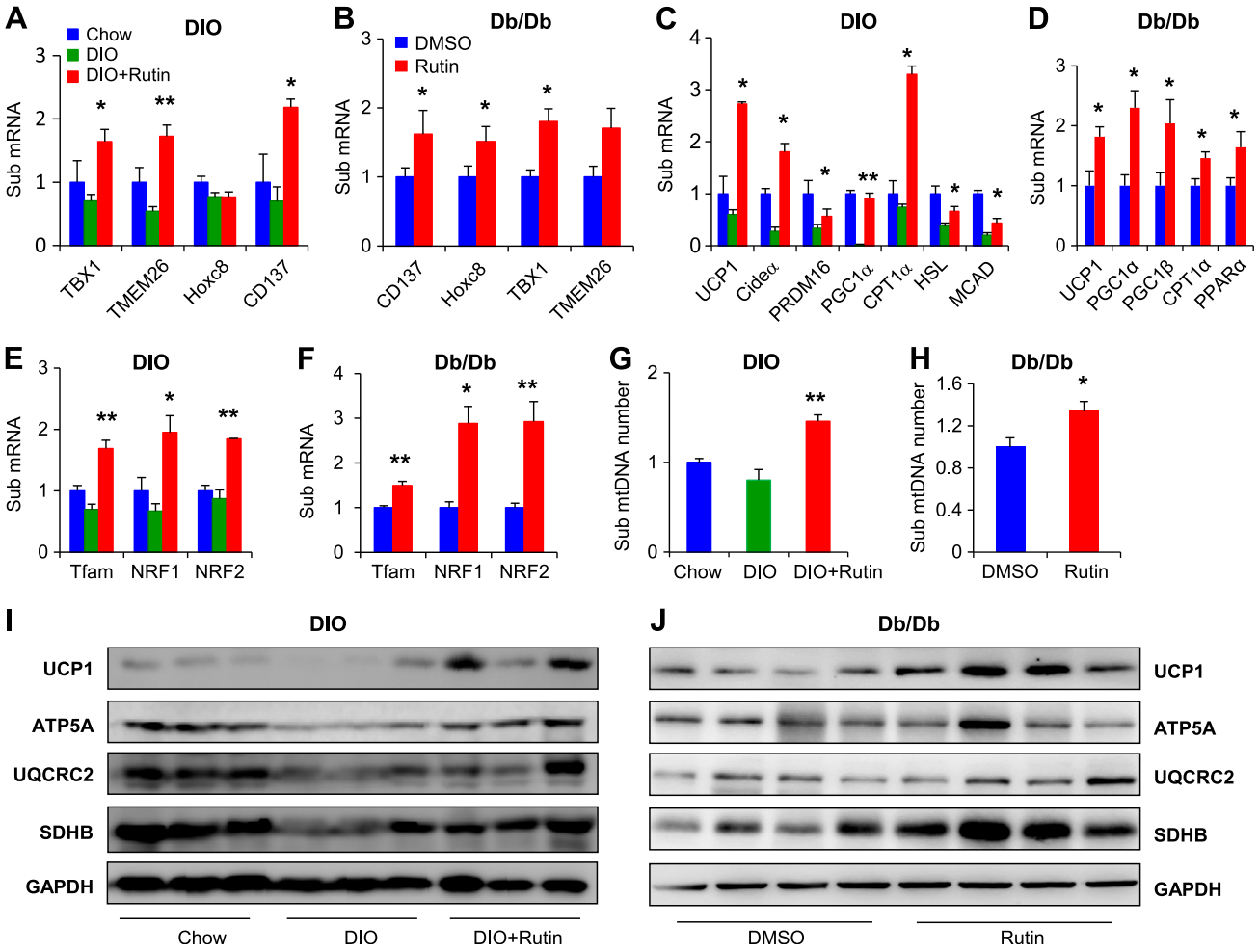

Figure 4. Rutin induces beige cell formation in subcutaneous fat. Rutin treatment significantly increases the expression levels of beige cell–specific genes (*A*, *B*), BAT thermogenic genes and fatty acid oxidation–related genes (*A*, *B*), mitochondria biogenic genes (*E*, *F*), and mitochondria copy number (*G*, *H*) in subcutaneous fat of DIO (*A*, *C*, *E*, *G*) and Db/Db (*B*, *D*, *F*, *H*) mice. Rutin increases UCP1 and mitochondrial oxphos complex proteins in subcutaneous fat of DIO (*I*) and Db/Db (*J*) mice. Data are means ± SEM ($n = 10$). $^*P < 0.05$, $^{**}P < 0.01$ *vs.* control.

SIRT1-mediated PGC1α deacetylation and activation are critical for mitochondrial function in BAT (27). Furthermore, SIRT1-activating compounds (STACs) enhance SIRT1 activity by deacetylation of its substrate, such as PGC1α (28). These previous results led us to investigate whether rutin-induced BAT activation is dependent on the SIRT1- PGC1α signaling pathway. The expression of SIRT1, PGC1α, and Tfam was significantly increased by rutin treatment in BAT (**Fig. 5*A*, *B***) and sWAT (Fig. 5*C*, *D*) from both DIO and Db/Db mouse models. These results indicate that rutin may affect SIRT1 protein stability. To this end, protein stability was examined by a cycloheximide assay. Our results showed that rutin treatment increased SIRT1 stability (Fig. 5*E*, *F*). Consistent with previous reports, SIRT1 deacetylated PGC1α, and rutin treatment substantially increased SIRT1-mediated PGC1α deacetylation (Fig. 5*G*), whereas knockdown SIRT1 diminished rutin-mediated PGC1α deacetylation (Fig. 5*H*). These results suggest that rutin increases SIRT1 deacetylase activity. To further investigate whether rutin affects SIRT1 deacetylase activity, an *in vitro* deacetylation assay was performed by using acetylated PGC1α as a substrate. Our results showed that rutin significantly increased the deacetylase activity of wild-type (WT) SIRT1, but not that of the mutant protein (E230K), which has been shown to be critical for activation by all previously reported chemically distinct STACs (28, 29) (Fig. 5*I*, *J*). These findings demonstrate that rutin increases SIRT1 stability and its deacetylase activity.

Rutin activates the SIRT1/PGC1α/Tfam signaling pathway

The remaining question was how rutin modulates SIRT1 activity. To investigate whether rutin increases SIRT1 deacetylase activity through direct binding, the energetic binding of rutin to purified SIRT1 protein was studied by ITC. Similar to the previously reported STACs (28), rutin alone did not show any detectable binding with SIRT1 protein (data not shown). However, it was found to be bound to WT SIRT1, but not to the mutant, only in the presence of acetylated peptide substrate p53 *in vitro* (**Fig. 6*A*, *B***). These results demonstrate that rutin directly binds to SIRT1 protein.

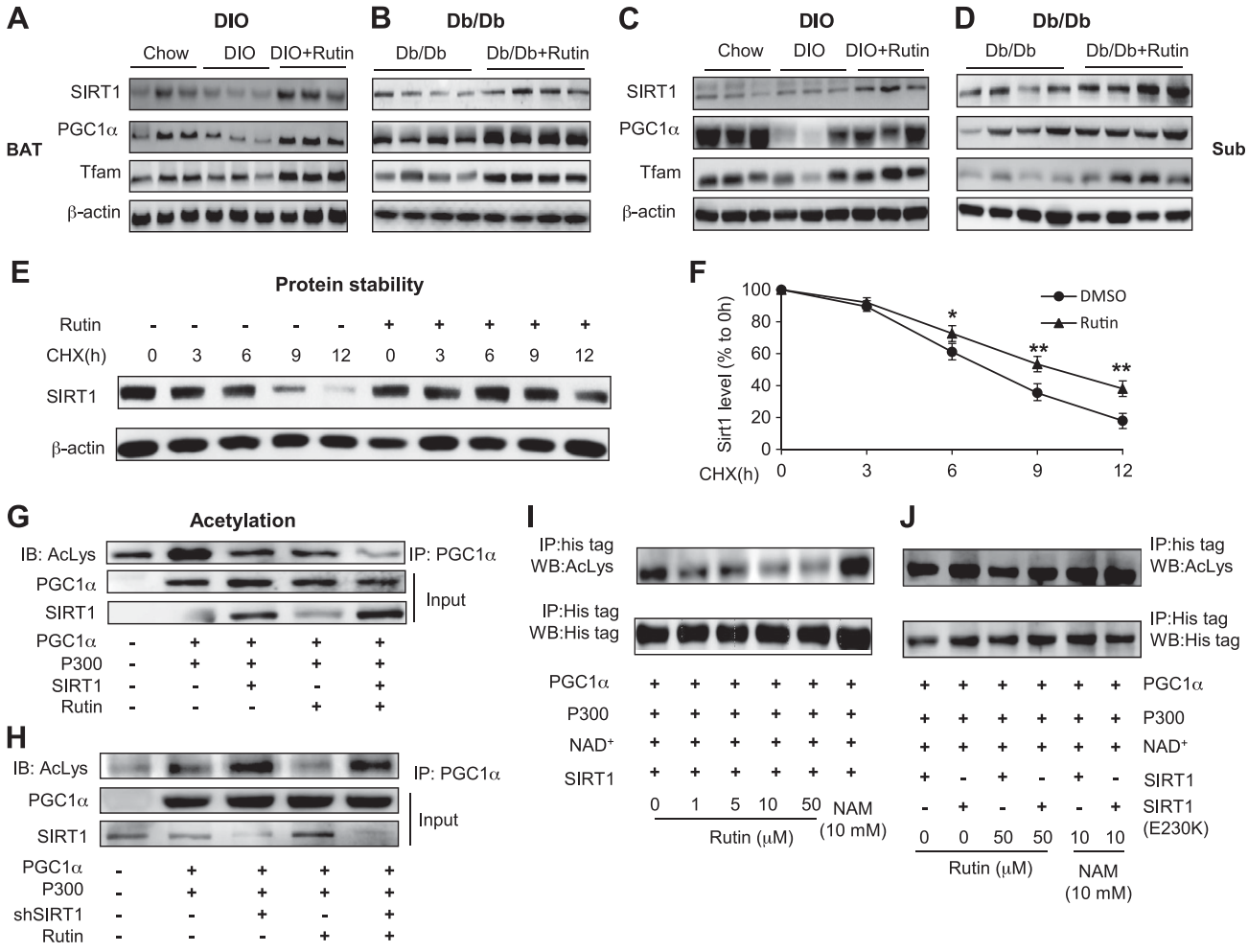

Figure 5. Rutin stabilizes SIRT1 and increases deacetylase activity. Rutin treatment increases SIRT1, PGC1α, and Tfam expression in BAT (*A*, *B*) and sWAT (*C*, *D*) of DIO (*A*, *C*) and Db/Db (*B*, *D*) mice. Rutin treatment increased SIRT1 protein stability (*E*, *F*). SIRT1 deacetylated PGC1α, and rutin treatment substantially increased SIRT1-mediated PGC1α deacetylation (*G*). In contrast, shSIRT1 treatment significantly diminished rutin-mediated PGC1α deacetylation (*H*). Rutin significantly increased deacetylase activity of WT SIRT1, not mutant SIRT1 (E230K) protein, *in vitro* (*I*, *J*). Data are means ± SEM ($n = 3$–6). $^*P < 0.05$, $^{**}P < 0.01$ *vs.* control.

Tfam is a key gene for mitochondrial DNA replication and biogenesis, and PGC1α regulates Tfam transcription by interacting with NRF1/2 (30). Coimmunoprecipitation analysis revealed that PGC1α interacted with NRF2, and this interaction was further enhanced by rutin treatment (Fig. 6*C*). To identify whether rutin could regulate NRF2-mediated Tfam transcriptional activation, a luciferase reporter assay was performed with the Tfam promoter where NRF2 binding sites have been characterized (31). As shown in Fig. 6*D*, PGC1α and NRF2 increased the expression of WT Tfam luciferase, whereas this activation was diminished by mutation of thNRF2 binding site in the Tfam promoter. Rutin treatment further increased PGC1α- and NRF2-mediated Tfam luciferase expression (Fig. 6*E*). Consistent with our hypothesis, rutin treatment dramatically increased the mitochondrial copy number in primary brown adipocytes from WT mice but not in SIRT1 KO mice (Fig. 6*F*). These results suggest that PGC1α and NRF2 form a transcriptional complex that regulates Tfam transcription in brown adipocytes. Taken together, these data show that rutin regulates Tfam transcription through a SIRT1/PGC1α/NRF2–dependent pathway (**Fig. 7**).

DISCUSSION

As a thermogenic organ, BAT has been known to be essential for maintaining the body temperature of rodents and infants (5, 32). Cold exposure is now believed to be the safest way of activating BAT through increasing thermogenic protein expression. Activated BAT after cold exposure promotes the clearance of excessive triglycerides in the plasma by increasing lipid uptake into BAT, subsequently improving energy metabolism and weight loss (33, 34). Under thermoneutral conditions, activated BAT was detected by a PET-CT scan in only 3.1% of men and 7.5% of women (9); however, it has been found in 96% of the population after cold exposure (10). BAT activity correlates inversely with body mass index in humans (9, 35) and BAT mass. Moreover, its activity progressively decreases with age (9, 33). Studies by our group and others

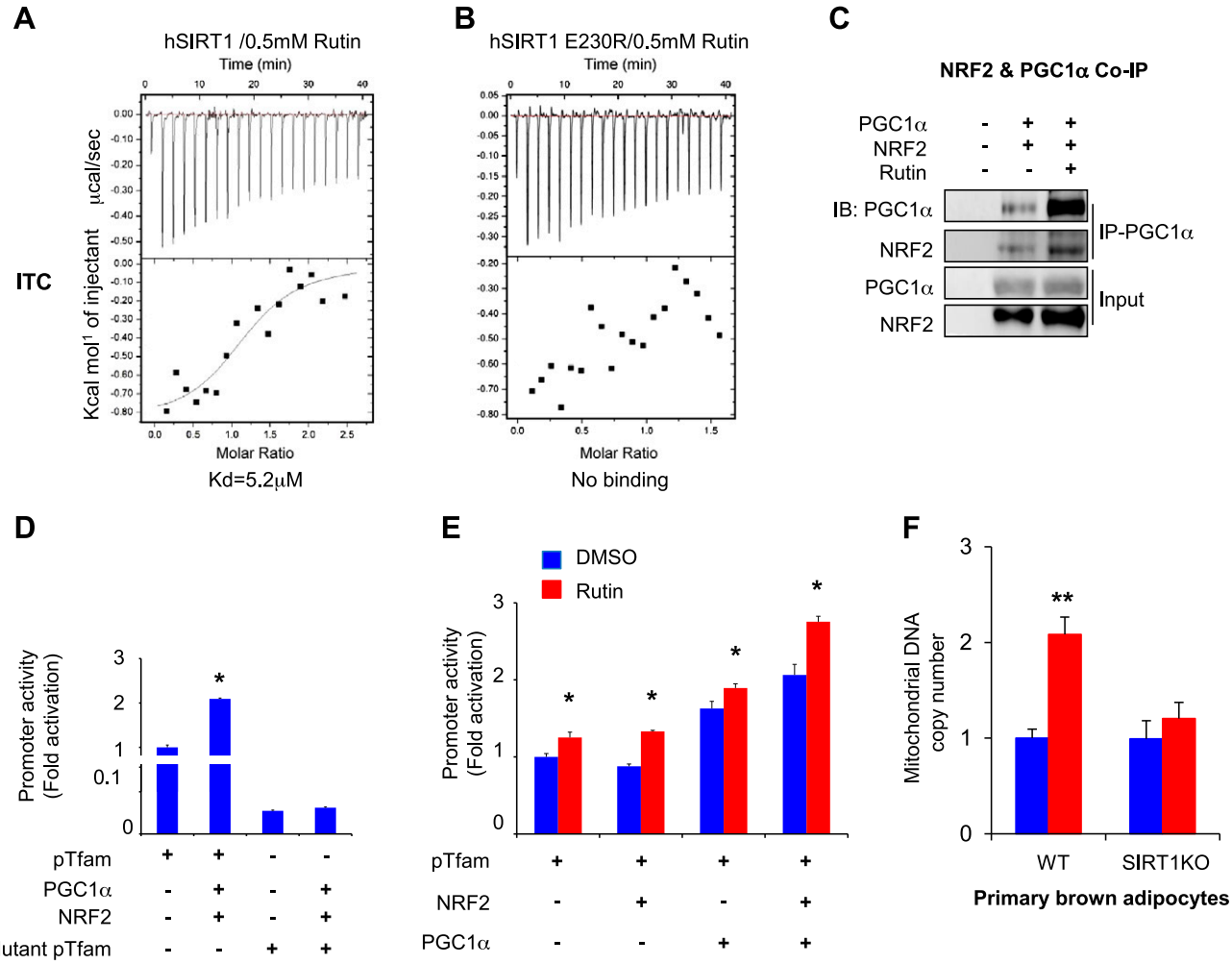

Figure 6. Rutin binds to SIRT1 protein. ITC results show that rutin binds only to WT SIRT1 (*A*), not to mutant SIRT1 protein (*B*), in the presence of acetylated peptide substrate p53 *in vitro*. Coimmunoprecipitation analysis reveals that PGC1α interacts with NRF2, and this interaction is further enhanced by rutin treatment (*C*). Rutin treatment further increases PGC1α- and NRF2-mediated WT, but not NRF2 binding site mutant Tfam luciferase expression (*D*, *E*). *F*) Rutin treatment significantly increased the number of mitochondria in WT but not in SIRT1 KO primary brown adipocytes. Data are means ± SEM ($n = 3$–6). $^{*}P < 0.05$, $^{**}P < 0.01$ *vs.* control.

have shown that BAT transplantation reverses metabolic disorders in various obese mouse models (37–39). These previous results suggest that functional BAT in adults may play important roles in systemic energy metabolism. Therefore, enhancement of energy expenditure by increasing BAT mass and its activity is offered as a promising strategy to treat obesity and diabetes. Except for WAT and BAT, the third adipose tissue is identified by browning of WAT, which is termed "beige cells" and has the similar functional characteristics of BAT (6). Even though rosiglitazone or β-adrenergic agonist treatment has been reported to promote the browning of WAT to beige adipocytes (34, 1), the unwanted side effects they caused have prevented their application in clinical practice. In the current study, rutin , a novel cold mimetic ameliorated obesity in Db/Db and DIO mice by increasing energy expenditure *via* increased BAT activity and induced beige formation in sWAT.

Recently, we have shown that mulberry extract which contains a large amount of C3G and rutin increases the number of mitochondria and O_2 consumption during brown adipogenesis *in vitro* (15). In line with our previous *in vitro* results, in the current study, rutin treatment profoundly increased BAT activity (Fig. 3*M*) in obese mouse models. Furthermore, BAT activation was more profound in Db/Db mice than in DIO mice, given that Db/Db mice had been known to be deficient in BAT activity (23, 24). Other studies have shown that rutin can reduce body weight gain and improve glucose homeostasis in rodent models (18, 41), but the underlying molecular mechanisms are still unclear. Given the variety of physiologic activity of rutin, we are optimistic that it can be used to activate BAT in a therapeutic view.

Accumulating evidence has demonstrated that BAT thermogenesis and white fat browning are critical strategies for antiobesity (40, 42). In the present study, rutin activated BAT and white fat browning (Figs. 3, 4). It has been demonstrated that thermogenesis is predominantly dependent on BAT in rodents (43). Moreover, rutin treatment increased the levels of thermogenic gene expression

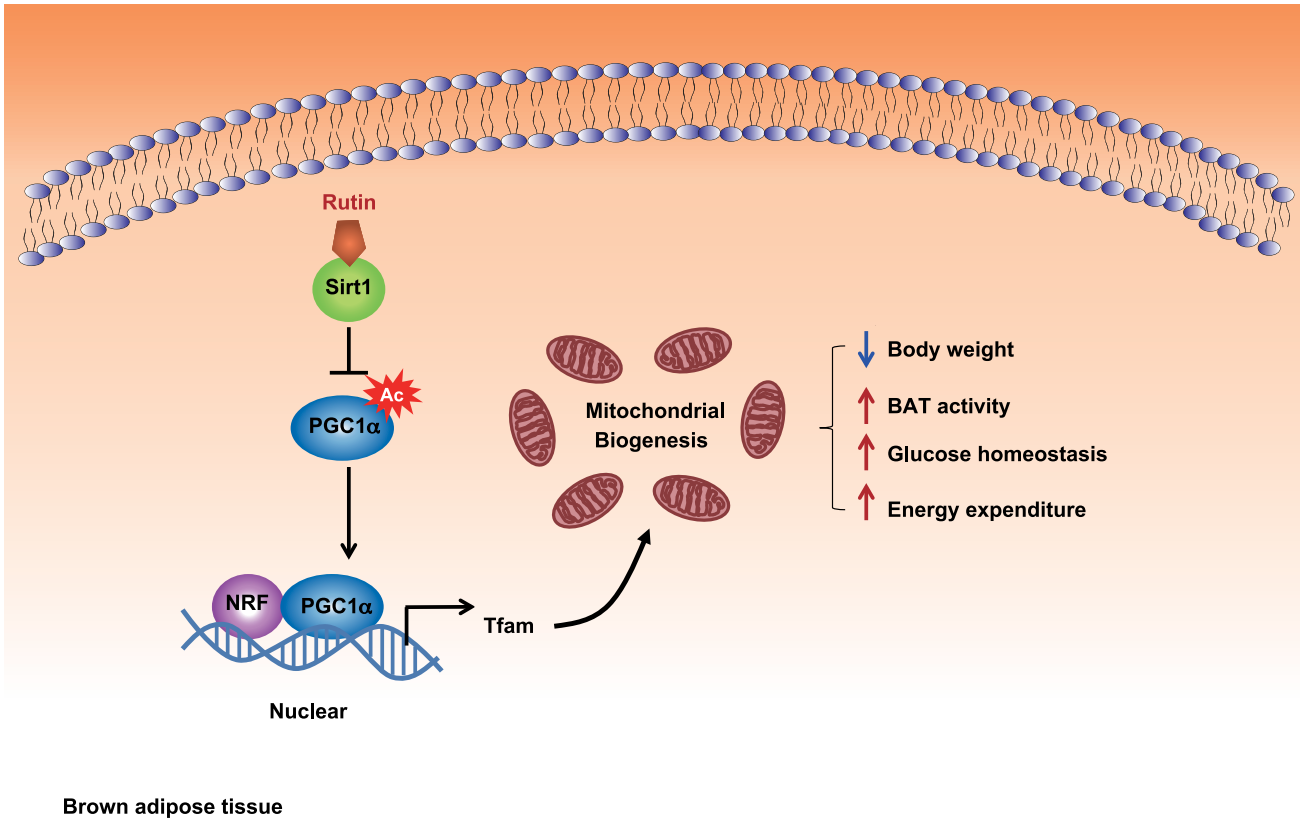

Figure 7. Rutin binds to SIRT1 protein and controls mitochondrial biogenesis. It binds and activates SIRT1, thereby increasing PGC1α activity, modulating Tfam transcriptional activity, and increasing mitochondrial biogenesis, resulting in increased BAT activity and adiposity reduction.

in sWAT of both obese mouse models (Fig. 3*C*, *D*, *I*, *J*). These findings strongly suggest that rutin has a white fat–browning effect. Rutin treatment significantly reduced body weight gain (Fig. 2*A*, *B*), by decreasing body fat accumulation (Fig.2*C*, *D* and data not shown).

It has been demonstrated that mitochondrial function has an impact on whole-body metabolism that is closely related to BAT function (6). In the present study, rutin treatment increased mitochondrial copy number and upregulated BAT-specific OXPHOS protein in BAT, indicating that it can improve mitochondrial function. Furthermore, rutin treatment improved energy expenditure (Fig. 2*E–H*) and glucose homeostasis (Fig. 2*M*, *N*) in both obese mouse models. In addition, rutin treatment enhanced adaptive thermogenic capacity (Fig. 2*I–L*). Altogether, our results indicate that the rutin-mediated increase in mitochondrial function and energy expenditure may synergistically contribute to favorable metabolic profiles against obesity and metabolic disorders.

SIRT1 is an NAD-dependent protein deacetylase (mammalian homolog of the yeast enzyme Sir2) that influences yeast lifespan (44). Recently, it has been shown that adipose tissue-specific overexpression of SIRT1 enhances whole-body energy metabolism and improves age-related insulin resistance in mice (45). In particular, moderate SIRT1 overexpression increases energy expenditure and improves glucose homeostasis by enhancing BAT function (46). In contrast, the adipose tissue–specific knockout of SIRT1 leads to increases in body weight gain and metabolic dysfunction (47). PGC1α is a master regulator of mitochondrial biogenesis (27) in mammals, and it has been reported to be positively regulated by SIRT1 (23). SIRT1 activation decreases PGC1α acetylation and also increases its activity (24). Several polyphenols from plant extract, including resveratrol, are known to directly stimulate BAT thermogenesis by increasing expression and activation of SIRT1 (48) and promote WAT browning by activating AMPK1 (9). In our study, rutin increased the stability of SIRT1 protein (Fig. 5*E*, *F*). Moreover, our results showed that rutin could increase SIRT1-mediated PGC1α deacetylation *in vivo* and *in vitro* (Fig. 5*G*, *I*), whereas knockdown of SIRT1 diminished rutin-mediated PGC1α deacetylation (Fig. 5*H*). Consistently, rutin treatment significantly increased PGC1α and Tfam expression in BAT (Fig. 5*A*, *B*) and sWAT (Fig. 5*C*, *D*) from both DIO and Db/Db mouse models. These results highlight that the rutin SIRT1/PGC1α/TFAM pathway is actively involved in BAT and beige cell function.

Although we cannot exclude the possibility that rutin regulates whole-body energy metabolism *via* enhancing BAT metabolic activity through stimulating the sympathetic nervous system (50), the cellular experiments indicated that rutin directly activated BAT oxidation *in vitro* (Fig. 1). In agreement with a report that BAT activation is associated with lipolysis (51), rutin treatment significantly increased the lipolysis in fully differentiated BAT cells

(Supplemental Fig. S5*C*). Moreover, we found that numerous genes involved in thermogenesis and fatty acid oxidation were upregulated in BAT and sWAT (Fig. 3*A–D*). These results suggest that rutin activates BAT activity *via* increasing lipolysis. In the current study, rutin bound to SIRT1 at Glu^{230} and dramatically increased SIRT1 activity, which led to hypoacetylation of PGC1α protein and upregulation of Tfam expression. However, the exact molecular mechanism underlying rutin-mediated SIRT1 activation remains to be further investigated.

CONCLUSIONS

In summary, the most notable finding of the present study is that rutin ameliorates obesity through BAT activation and beige formation in sWAT. In particular, rutin, as a SIRT1 activator, contributes to activation of the SIRT1/PGC1α/Tfam–signaling cascade and thereby the number of mitochondria and BAT activity, as well as energy expenditure, resulting in a significant reduction in adiposity. It has been used clinically as a capillary stabilizer for more than 60 yr without any side effects (52). Therefore, rutin, as a cold mimetic, may open a novel avenue for the treatment of obesity and its related diseases. FJ

ACKNOWLEDGMENTS

The authors thank Dr. Ruiming Xu [Institute of Biophysics, Chinese Academy of Sciences (CAS)] for generously providing us with the SIRT1 proteins. This work was supported by the Strategic Priority Research Program XDB13030000 (to W.J.); Key Research Program KJZD-EW-L01-3 (to W.J.); CAS, One Hundred Talents Program of the CAS (to W.J.); Ministry of Science and Technology of China Grants 2012CBA01301, 2015CB943102, and 2012CB944701 (to W.J.); National Natural Science Foundation of China Grants 31171131 and 81370951 (to W.J.); National Basic Research Program of China Grants 2012CB910701 and 2013DFA31990 (to Z.Y.); National Natural Science Foundation of China Grant 81500659 (to X.L); Beijing Municipal Administration of Hospitals Grant ZYLX201402 (to J.C.); National "Twelfth Five-Year" Plan for Science and Technology Support Grants 2012BAD31B07 and 2012BAD31B05 (to W.H.); and Special Fund for Agro-scientific Research in the Public Interest Grant 201303073-2 (to J.Z.). The authors declare no conflicts of interest.

AUTHOR CONTRIBUTIONS

W. Jin., Z. Yuan., and J. Cheng. designed the research; X. Yuan., G. Wei., Y. You, Y. Huang, H. J. Lee, M. Dong, J. Lin, T. Hu, H. Zhang, C. Zhang, H. Zhou, R. Ye, X. Qi, S. Liu, W. Xie, Q. Liu, B. Zhai, J. Zhai, W. Huang, C. Cui, D. Li, and X. Liu, performed the research; X. Yuan, G. Wei, Y. You, . J. Cheng, Z. Yuan, and W. Jin analyzed the data; and X. Yuan, G. Wei, Y. You, H. J. Lee, C. J., Z. Yuan. and W. Jin wrote the paper.

REFFERENCES

1. Jin, W., and Patti, M. E. (2009) Genetic determinants and molecular pathways in the pathogenesis of type 2 diabetes. *Clin. Sci.* **116**, 99–111
2. Lowell, B. B., and Spiegelman, B. M. (2000) Towards a molecular understanding of adaptive thermogenesis. *Nature* **404**, 652–660
3. Ravussin, E., and Galgani, J. E. (2011) The implication of brown adipose tissue for humans. *Annu. Rev. Nutr.* **31**, 33–47
4. Tseng, Y. H., Cypess, A. M., and Kahn, C. R. (2010) Cellular bioenergetics as a target for obesity therapy. *Nat. Rev. Drug Discov.* **9**, 465–482
5. Cannon, B., and Nedergaard, J. (2004) Brown adipose tissue: function and physiological significance. *Physiol. Rev.* **84**, 277–359
6. Harms, M., and Seale, P. (2013) Brown and beige fat: development, function and therapeutic potential. *Nat. Med.* **19**, 1252–1263
7. Matsushita, M., Yoneshiro, T., Aita, S., Kameya, T., Sugie, H., and Saito, M. (2014) Impact of brown adipose tissue on body fatness and glucose metabolism in healthy humans. *Int. J. Obes. (Lond.)* **38**, 812–817
8. Kajimura, S., Spiegelman, B. M., and Seale, P. (2015) Brown and beige fat: physiological roles beyond heat generation. *Cell Metab.* **22**, 546–559
9. Cypess, A. M., Lehman, S., Williams, G., Tal, I., Rodman, D., Goldfine, A. B., Kuo, F. C., Palmer, E. L., Tseng, Y. H., Doria, A., Kolodny, G. M., and Kahn, C. R. (2009) Identification and importance of brown adipose tissue in adult humans. *N. Engl. J. Med.* **360**, 1509–1517
10. Van Marken Lichtenbelt, W. D., Vanhommerig, J. W., Smulders, N. M., Drossaerts, J. M. A. F. L., Kemerink, G. J., Bouvy, N. D., Schrauwen, P., and Teule, G. J. J. (2009) Cold-activated brown adipose tissue in healthy men. *N. Engl. J. Med.* **360**, 1500–1508
11. Virtanen, K. A., Lidell, M. E., Orava, J., Heglind, M., Westergren, R., Niemi, T., Taittonen, M., Laine, J., Savisto, N. J., Enerbäck, S., and Nuutila, P. (2009) Functional brown adipose tissue in healthy adults. *N. Engl. J. Med.* **360**, 1518–1525; correction **361**, 1123
12. Wu, J., Boström, P., Sparks, L. M., Ye, L., Choi, J. H., Giang, A. H., Khandekar, M., Virtanen, K. A., Nuutila, P., Schaart, G., Huang, K., Tu, H., van Marken Lichtenbelt, W. D., Hoeks, J., Enerbäck, S., Schrauwen, P., and Spiegelman, B. M. (2012) Beige adipocytes are a distinct type of thermogenic fat cell in mouse and human. *Cell* **150**, 366–376
13. Boström, P., Wu, J., Jedrychowski, M. P., Korde, A., Ye, L., Lo, J. C., Rasbach, K. A., Boström, E. A., Choi, J. H., Long, J. Z., Kajimura, S., Zingaretti, M. C., Vind, B. F., Tu, H., Cinti, S., Højlund, K., Gygi, S. P., and Spiegelman, B. M. (2012) A PGC1-α-dependent myokine that drives brown-fat-like development of white fat and thermogenesis. *Nature* **481**, 463–468
14. Seale, P., Conroe, H. M., Estall, J., Kajimura, S., Frontini, A., Ishibashi, J., Cohen, P., Cinti, S., and Spiegelman, B. M. (2011) Prdm16 determines the thermogenic program of subcutaneous white adipose tissue in mice. *J. Clin. Invest.* **121**, 96–105
15. You, Y., Yuan, X., Lee, H. J., Huang, W., Jin, W., and Zhan, J. (2015) Mulberry and mulberry wine extract increase the number of mitochondria during brown adipogenesis. *Food Funct.* **6**, 401–408
16. Korkmaz, A., and Kolankaya, D. (2010) Protective effect of rutin on the ischemia/reperfusion induced damage in rat kidney. *J. Surg. Res.* **164**, 309–315
17. Stanley Mainzen Prince, P., and Kamalakkannan, N. (2006) Rutin improves glucose homeostasis in streptozotocin diabetic tissues by altering glycolytic and gluconeogenic enzymes. *J. Biochem. Mol. Toxicol.* **20**, 96–102
18. Gao, M., Ma, Y., and Liu, D. (2013) Rutin suppresses palmitic acids-triggered inflammation in macrophages and blocks high fat diet-induced obesity and fatty liver in mice. *Pharm. Res.* **30**, 2940–2950
19. Chi, Q. S., and Wang, D. H. (2011) Thermal physiology and energetics in male desert hamsters (Phodopus roborovskii) during cold acclimation. *J. Comp. Physiol. B.* **181**, 91-103
20. Liu, X., Zheng, Z., Zhu, X., Meng, M., Li, L., Shen, Y., Chi, Q., Wang, D., Zhang, Z., Li, C., Li, Y., Xue, Y., Speakman, J. R., and Jin, W. (2013) Brown adipose tissue transplantation improves whole-body energy metabolism. *Cell Res.* **23**, 851–854
21. Li, R., Guan, H., and Yang, K. (2012) Neuropeptide Y potentiates beta-adrenergic stimulation of lipolysis in 3T3-L1 adipocytes. *Regul. Pept.* **178**, 16–20
22. Sleeman, M. W., Garcia, K., Liu, R., Murray, J. D., Malinova, L., Moncrieffe, M., Yancopoulos, G. D., and Wiegand, S. J. (2003) Ciliary neurotrophic factor improves diabetic parameters and hepatic steatosis and increases basal metabolic rate in db/db mice. *Proc. Natl. Acad. Sci. USA* **100**, 14297–14302
23. Hossain, P., Kawar, B., and El Nahas, M. (2007) Obesity and diabetes in the developing world: a growing challenge. *N. Engl. J. Med.* **356**, 213–215
24. Trayhurn, P. (1979) Thermoregulation in the diabetic-obese (db/db) mouse: the role of non-shivering thermogenesis in energy balance. *Pflugers Arch.* **380**, 227–232

25. Lončar, D., Bedrica, L., Mayer, J., Cannon, B., Nedergaard, J., Afzelius, B. A., and Svajger, A. (1986) The effect of intermittent cold treatment on the adipose tissue of the cat: apparent transformation from white to brown adipose tissue. *J. Ultrastruct. Mol. Struct. Res.* **97**, 119–129
26. Rodgers, J. T., Lerin, C., Haas, W., Gygi, S. P., Spiegelman, B. M., and Puigserver, P. (2005) Nutrient control of glucose homeostasis through a complex of PGC-1alpha and SIRT1. *Nature* **434**, 113–118
27. Lagouge, M., Argmann, C., Gerhart-Hines, Z., Meziane, H., Lerin, C., Daussin, F., Messadeq, N., Milne, J., Lambert, P., Elliott, P., Geny, B., Laakso, M., Puigserver, P., and Auwerx, J. (2006) Resveratrol improves mitochondrial function and protects against metabolic disease by activating SIRT1 and PGC-1alpha. *Cell* **127**, 1109–1122
28. Hubbard, B. P., Gomes, A. P., Dai, H., Li, J., Case, A. W., Considine, T., Riera, T. V., Lee, J. E., e, S. Y., Lamming, D. W., Pentelute, B. L., Schuman, E. R., Stevens, L. A., Ling, A. J., Armour, S. M., Michan, S., Zhao, H., Jiang, Y., Sweitzer, S. M., Blum, C. A., Disch, J. S., Ng, P. Y., Howitz, K. T., Rolo, A. P., Hamuro, Y., Moss, J., Perni, R. B., Ellis, J. L., Vlasuk, G. P., and Sinclair, D. A. (2013) Evidence for a common mechanism of SIRT1 regulation by allosteric activators. *Science* **339**, 1216–1219
29. Cao, D., Wang, M., Qiu, X., Liu, D., Jiang, H., Yang, N., and Xu, R. M. (2015) Structural basis for allosteric, substrate-dependent stimulation of SIRT1 activity by resveratrol. *Genes Dev.* **29**, 1316–1325
30. Wu, Z., Puigserver, P., Andersson, U., Zhang, C., Adelmant, G., Mootha, V., Troy, A., Cinti, S., Lowell, B., Scarpulla, R. C., and Spiegelman, B. M. (1999) Mechanisms controlling mitochondrial biogenesis and respiration through the thermogenic coactivator PGC-1. *Cell* **98**, 115–124
31. Larsson, N. G., Barsh, G. S., and Clayton, D. A. (1997) Structure and chromosomal localization of the mouse mitochondrial transcription factor A gene (Tfam). *Mamm. Genome* **8**, 139–140
32. Zingaretti, M. C., Crosta, F., Vitali, A., Guerrieri, M., Frontini, A., Cannon, B., Nedergaard, J., and Cinti, S. (2009) The presence of UCP1 demonstrates that metabolically active adipose tissue in the neck of adult humans truly represents brown adipose tissue. *FASEB J.* **23**, 3113–3120
33. Bartelt, A., Bruns, O. T., Reimer, R., Hohenberg, H., Ittrich, H., Peldschus, K., Kaul, M. G., Tromsdorf, U. I., Weller, H., Waurisch, C., Eychmüller, A., Gordts, P. L., Rinninger, F., Bruegelmann, K., Freund, B., Nielsen, P., Merkel, M., and Heeren, J. (2011) Brown adipose tissue activity controls triglyceride clearance. *Nat. Med.* **17**, 200–205
34. Yoneshiro, T., Aita, S., Matsushita, M., Kayahara, T., Kameya, T., Kawai, Y., Iwanaga, T., and Saito, M. (2013) Recruited brown adipose tissue as an antiobesity agent in humans. *J. Clin. Invest.* **123**, 3404–3408
35. Saito, M., Okamatsu-Ogura, Y., Matsushita, M., Watanabe, K., Yoneshiro, T., Nio-Kobayashi, J., Iwanaga, T., Miyagawa, M., Kameya, T., Nakada, K., Kawai, Y., and Tsujisaki, M. (2009) High incidence of metabolically active brown adipose tissue in healthy adult humans: effects of cold exposure and adiposity. *Diabetes* **58**, 1526–1531
36. Pfannenberg, C., Werner, M. K., Ripkens, S., Stef, I., Deckert, A., Schmadl, M., Reimold, M., Häring, H. U., Claussen, C. D., and Stefan, N. (2010) Impact of age on the relationships of brown adipose tissue with sex and adiposity in humans. *Diabetes* **59**, 1789–1793
37. Liu, X., Wang, S., You, Y., Meng, M., Zheng, Z., Dong, M., Lin, J., Zhao, Q., Zhang, C., Yuan, X., Hu, T., Liu, L., Huang, Y., Zhang, L., Wang, D., Zhan, J., Jong Lee, H., Speakman, J. R., and Jin, W. (2015) Brown adipose tissue transplantation reverses obesity in Ob/Ob mice. *Endocrinology* **156**, 2461–2469
38. Liu, X., Zheng, Z., Zhu, X., Meng, M., Li, L., Shen, Y., Chi, Q., Wang, D., Zhang, Z., Li, C., Li, Y., Xue, Y., Speakman, J. R., and Jin, W. (2013) Brown adipose tissue transplantation improves whole-body energy metabolism. *Cell Res.* **23**, 851–854
39. Stanford, K. I., Middelbeek, R. J., Townsend, K. L., An, D., Nygaard, E. B., Hitchcox, K. M., Markan, K. R., Nakano, K., Hirshman, M. F., Tseng, Y. H., and Goodyear, L. J. (2013) Brown adipose tissue regulates glucose homeostasis and insulin sensitivity. *J. Clin. Invest.* **123**, 215–223
40. Cypess, A. M., Chen, Y. C., Sze, C., Wang, K., English, J., Chan, O., Holman, A. R., Tal, I., Palmer, M. R., Kolodny, G. M., and Kahn, C. R. (2012) Cold but not sympathomimetics activates human brown adipose tissue in vivo. *Proc. Natl. Acad. Sci. USA* **109**, 10001–10005
41. Hsu, C. L., Wu, C. H., Huang, S. L., and Yen, G. C. (2009) Phenolic compounds rutin and o-coumaric acid ameliorate obesity induced by high-fat diet in rats. *J. Agric. Food Chem.* **57**, 425–431
42. Whittle, A. J., Carobbio, S., Martins, L., Slawik, M., Hondares, E., Vázquez, M. J., Morgan, D., Csikasz, R. I., Gallego, R., Rodriguez-Cuenca, S., Dale, M., Virtue, S., Villarroya, F., Cannon, B., Rahmouni, K., López, M., and Vidal-Puig, A. (2012) BMP8B increases brown adipose tissue thermogenesis through both central and peripheral actions. *Cell* **149**, 871–885
43. Shabalina, I. G., Petrovic, N., de Jong, J. M., Kalinovich, A. V., Cannon, B., and Nedergaard, J. (2013) UCP1 in brite/beige adipose tissue mitochondria is functionally thermogenic. *Cell Rep.* **5**, 1196–1203
44. Qiang, L., Wang, L., Kon, N., Zhao, W., Lee, S., Zhang, Y., Rosenbaum, M., Zhao, Y., Gu, W., Farmer, S. R., and Accili, D. (2012) Brown remodeling of white adipose tissue by SirT1-dependent deacetylation of Pparγ. *Cell* **150**, 620–632
45. Xu, C., Bai, B., Fan, P., Cai, Y., Huang, B., Law, I. K., Liu, L., Xu, A., Tung, C., Li, X., Siu, F. M., Che, C. M., Vanhoutte, P. M., and Wang, Y. (2013) Selective overexpression of human SIRT1 in adipose tissue enhances energy homeostasis and prevents the deterioration of insulin sensitivity with ageing in mice. *Am. J. Transl. Res.* **5**, 412–426
46. Boutant, M., Joffraud, M., Kulkarni, S. S., García-Casarrubios, E., García-Roves, P. M., Ratajczak, J., Fernández-Marcos, P. J., Valverde, A. M., Serrano, M., and Cantó, C. (2014) SIRT1 enhances glucose tolerance by potentiating brown adipose tissue function. *Mol. Metab.* **4**, 118–131
47. Chalkiadaki, A., and Guarente, L. (2012) High-fat diet triggers inflammation-induced cleavage of SIRT1 in adipose tissue to promote metabolic dysfunction. *Cell Metab.* **16**, 180–188
48. Andrade, J. M., Frade, A. C., Guimarães, J. B., Freitas, K. M., Lopes, M. T., Guimarães, A. L., de Paula, A. M., Coimbra, C. C., and Santos, S. H. (2014) Resveratrol increases brown adipose tissue thermogenesis markers by increasing SIRT1 and energy expenditure and decreasing fat accumulation in adipose tissue of mice fed a standard diet. *Eur. J. Nutr.* **53**, 1503–1510
49. Wang, S., Liang, X., Yang, Q., Fu, X., Rogers, C. J., Zhu, M., Rodgers, B. D., Jiang, Q., Dodson, M. V., and Du, M. (2015) Resveratrol induces brown-like adipocyte formation in white fat through activation of AMP-activated protein kinase (AMPK) alpha1. *Int. J. Obes. (Lond)* **39**, 967–978
50. Bartness, T. J., Vaughan, C. H., and Song, C. K. (2010) Sympathetic and sensory innervation of brown adipose tissue. *Int. J. Obes. (2005)* **34** (Suppl 1), S36–S42
51. Liew, C. W., Boucher, J., Cheong, J. K., Vernochet, C., Koh, H. J., Mallol, C., Townsend, K., Langin, D., Kawamori, D., Hu, J., Tseng, Y. H., Hellerstein, M. K., Farmer, S. R., Goodyear, L., Doria, A., Blüher, M., Hsu, S. I., and Kulkarni, R. N. (2013) Ablation of TRIP-Br2, a regulator of fat lipolysis, thermogenesis and oxidative metabolism, prevents diet-induced obesity and insulin resistance. *Nat. Med.* **19**, 217–226
52. Ozawa, H., Abiko, Y., and Akimoto, T. (2003) [A 50-year history of new drugs in Japan-the development and trends of hemostatics and antithrombotic drugs] (in Japanese). *Yakushigaku Zasshi* **38**, 93–105

Received for publication April 28, 2016.
Accepted for publication September 28, 2016.

Rutin ameliorates obesity through brown fat activation

Xiaoxue Yuan, Gang Wei, Yilin You, et al.

FASEB J published online October 20, 2016
Access the most recent version at doi:10.1096/fj.201600459RR

Table S1

Plasma profiles

	Db/Db+DMSO	Db/Db+Rutin	Chow	DIO	DIO+Rutin
CHO (mM)	3.65 ± 0.17	2.65 ± 0.12 *	2.8±0.18^{c}	4±0.16^{a}	3.62±0.07^{b}
TG (mM)	1.40 ± 0.12	1.16 ± 0.04 *	0.7±0.06^{c}	1.14±0.07^{a}	0.95±0.05^{b}
LDL (mM)	0.26 ± 0.01	0.21 ± 0.02	0.32±0.05^{bc}	0.57±0.02^{a}	0.50±0.02^{b}
HDL (mM)	3.01 ± 0.30	3.07 ± 0.24	2.70±0.08^{b}	3.63±0.08^{a}	3.42±0.07^{a}

Table S2

Primer Sequences

Primer	Forward	Reverse
AP2	GAAGACTGCGAGGACCTC	GAAGTGCCGTAATCCCCACAC
ATGL	ATATCCCACTTTAGCTCCAAGG	CAAGTTGTCTGAAATGCCGC
CEBP/α	GCGGGAACGCAACAACATC	GTCACTGGTCAACTCCAGCAC
CEBP/β	TGACGCAACACACGTGTAACTG	AACAACCCCGCAGGAACAT
CEBP/δ	CGACTTCAGCGCCTACATTGA	GAAGAGGTCGGCGAAGAGTT
Cideα	TGCTCTTCTGTATCGCCCAGT	GCCGTGTTAAGGAATCTGCTG
COX-II	GCCGACTAAATCAAGCAACA	CAATGGGCATAAAGCTATGG
CPT1α	GACTCCGCTCGCTCATTCC	GACTGTGAACTGGAAGGCCA
CyclophilinA	CAAATGCTGGACCAAACACA	GCCATCCAGCCATTCAGTCT
GCK	CTTCACCTTCTCCTTCCCTG	ATCTCAAAGTCCCCTCTCCT
HSL	CTGAGATTGAGGTGCTGTCG	CAAGGGAGGTGAGATGGTAAC
Il-6	AGACAAAGCCAGAGTCCTTCAG	GCCACTCCTTCTGTGACTCCAG
MCAD	ACTCGAAAGCGGCTCACAA	ACGGGGATAATCTCCTCTCTGG
MCP1	GTCCCTGTCATGCTTCTGG	GCTCTCCAGCCTACTCATTG
NRF1	CAACAGGGAAGAAACGGAAA	GCACCACATTCTCCAAAGGT
NRF2	TAGATGACCATGAGTCGCTTGC	GCCAAACTTGCTCCATGTCC
PGC1α	ACAGCTTTCTGGGTGGATT	TGAGGACCGCTAGCAAGTTT
PGC1β	CGTATTTGAGGACAGCAGCA	TACTGGGTGGGCTCTGGTAG
PPARα	AGCCTCAGCCAAGTTGAAGT	TGGGGAGAGAGGACAGATGG
PPARγ2	TCGCTGATGCACTGCCTATG	GAGAGGTCCACAGAGCTGATT
PRDM16	GAAGTCACAGGAGGACACGG	CTCGCTCCTCAACACACCTC
Tfam	GTCCATAGGCACCGTATTGC	CCCATGCTGGAAAAACACTT
TNFα	TGGGCCTCTCATGCACCACC	GAGGCAACCTGACCACTCTCCCT
UCP1	GGCAAAAACAGAAGGATTGC	TAAGCCGGCTGAGATCTTGT
β-globin	GAAGCGATTCTAGGGAGCAG	GGAGCAGCGATTCTGAGTAG

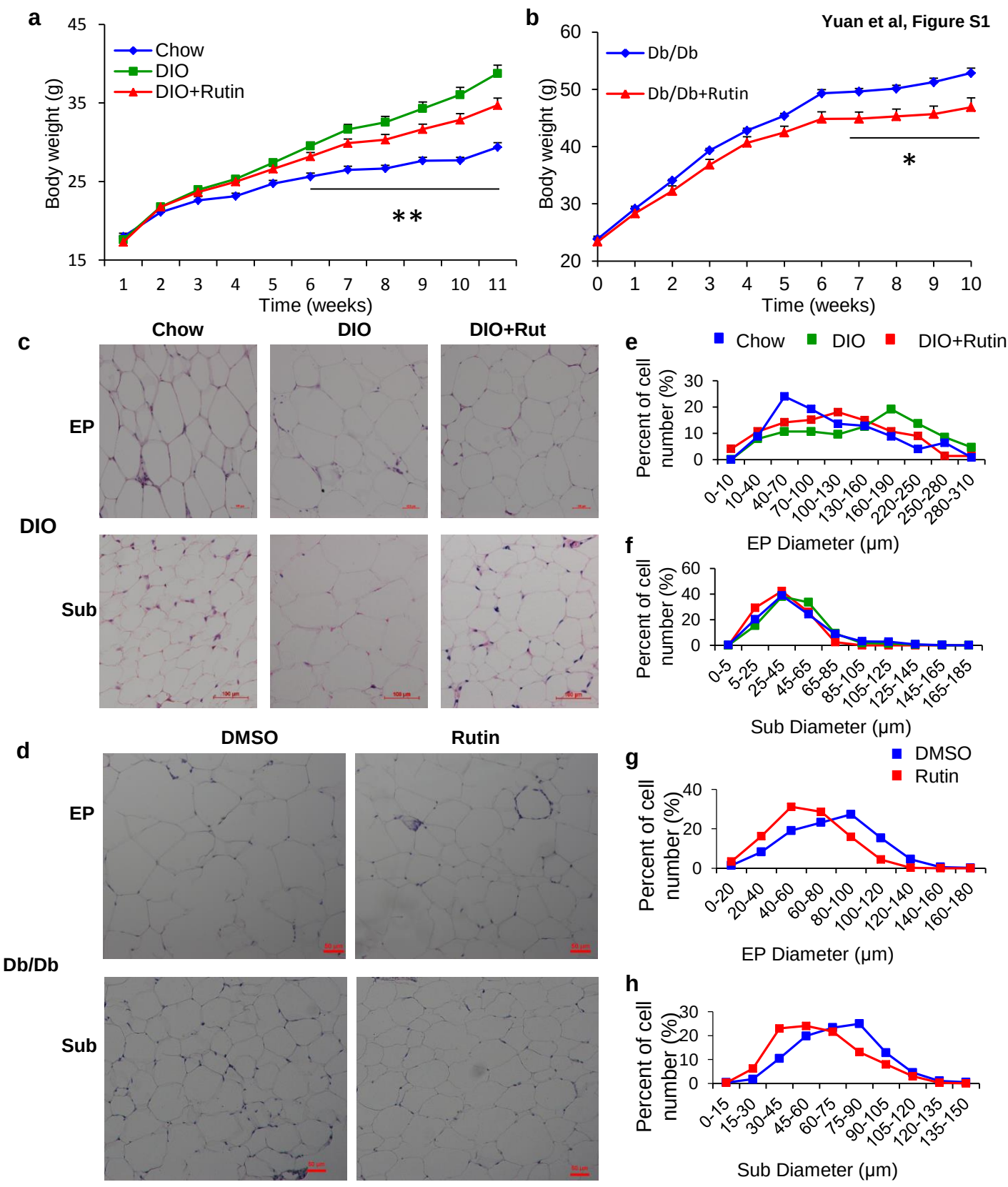

Supplementary Fig.1 Rutin decreases adipose tissue hypertrophy

a-b) Rutin protect against body weight gain in DIO obese mice (a) and Db/Db mice (b). c-d) Representative hematoxylin-eosin staining of inguinal WAT and epididymal WAT sections from DIO mice(c) and Db/Db mice(d) treated with DMSO or Rutin for 10 weeks (n=10). e-h) The size of adipocyte in epididymal fat and subcutaneous fat of DIO mice(e-f) and Db/Db mice(g-h) treated with DMSO or Rutin for 10 weeks (n=10). Data are represented as mean ± SEM. N=10. **: $P < 0.01$, *: $P < 0.05$ versus control.

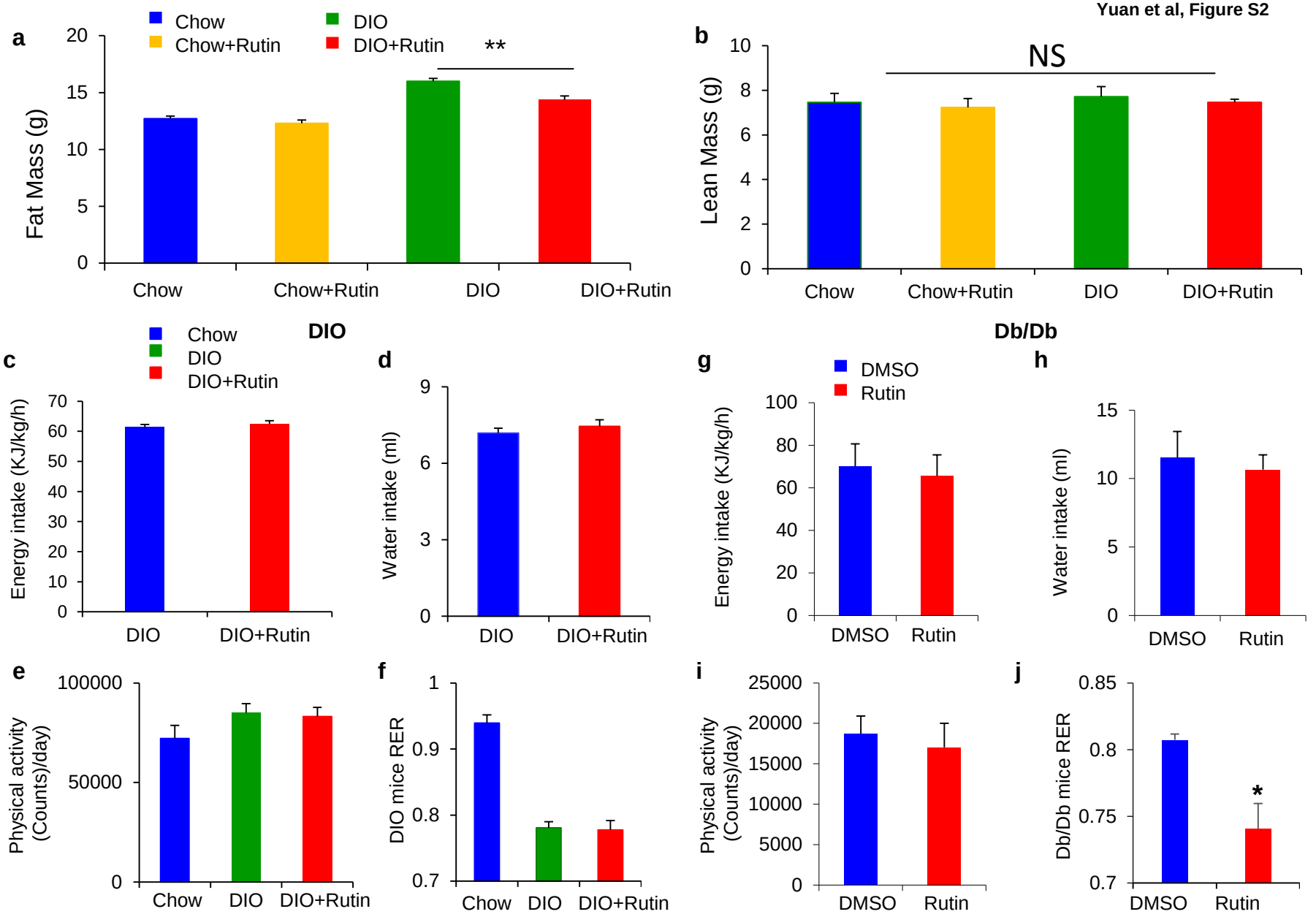

Supplementary Fig.2 Rutin treatment decreases adiposity

a-b) The total fat (a) and lean (b) mass was measured using MesoQMR after 7 weeks treatment during chow diet or high fat diet. Energy intake (c, g), water intake (d, h), Physical activity (e, i) and respiratory exchange ratio (RER) (f, j) of DIO mice(c-f) and Db/Db mice(g-j). Data are represented as mean ± SEM. **: $P < 0.01$, *: $P < 0.05$ versus control.

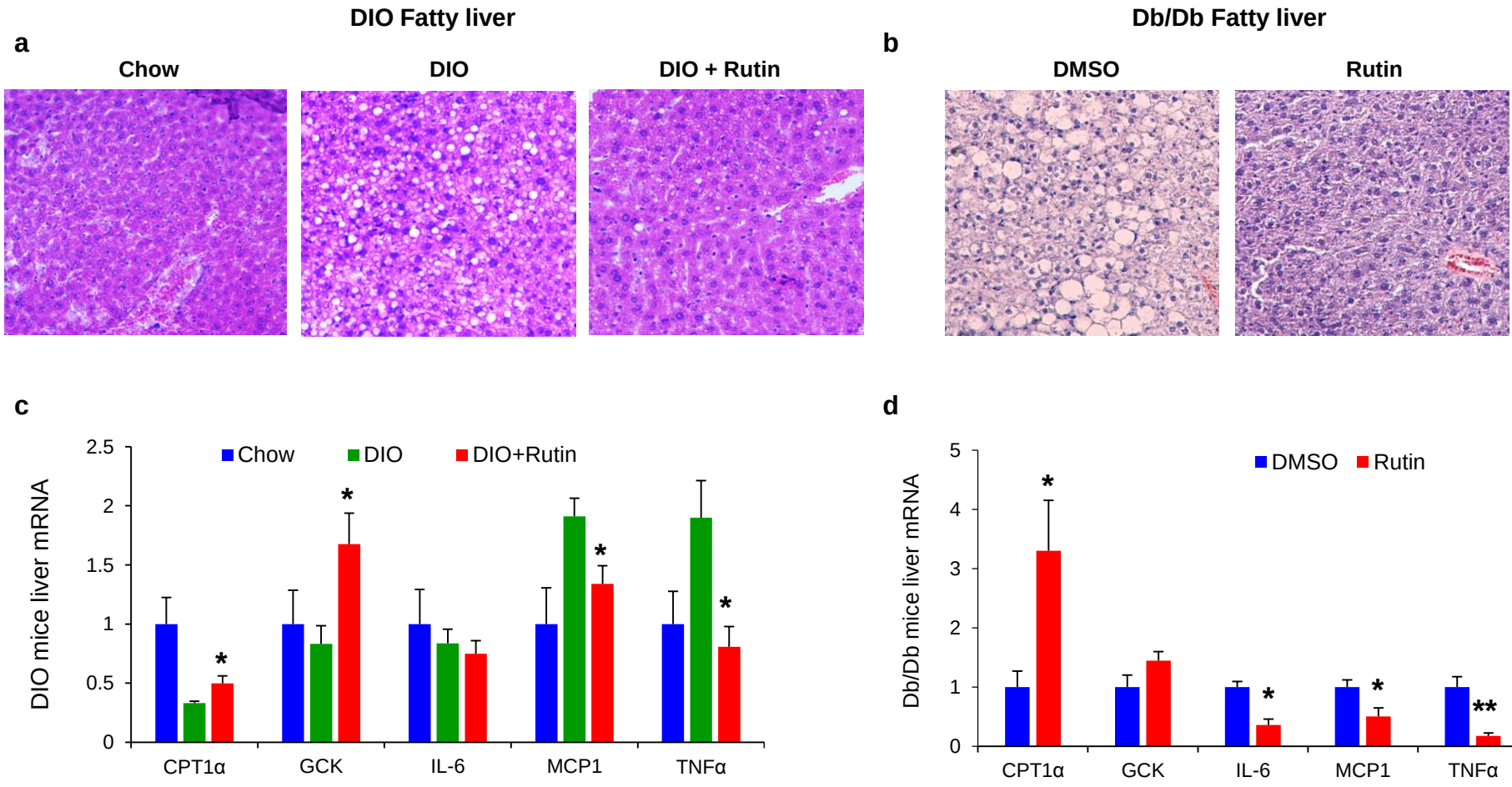

Supplementary Fig.3 Rutin treatment reverses hepatic steatosis

a-b) Representative hematoxylin-eosin staining of liver tissues from DIO mice (a) and Db/Db mice (b) treated with DMSO or Rutin for 10 weeks (n=10). c-d) Gene expression levels of liver from DIO mice (c) and Db/Db mice (d) treated with DMSO or Rutin for 10 weeks (n=10). Data are represented as mean ± SEM. . **: $P < 0.01$, *: $P < 0.05$ versus control.

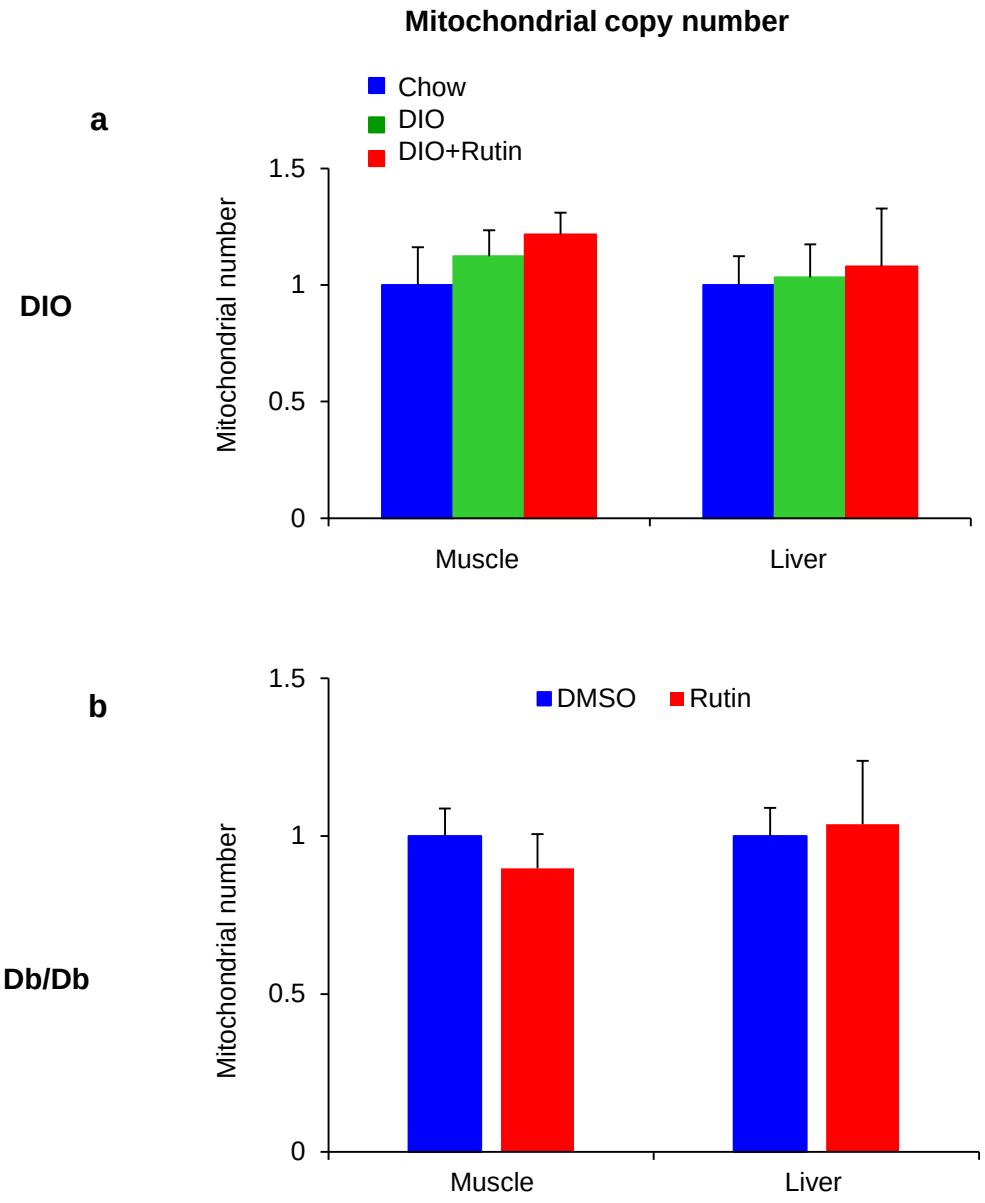

Supplementary Fig.4 Mitochondrial copy number.

a-b)There is no difference in mitochondrial copy number in muscle and liver tissues of DIO mice (a) and Db/Db mice (b) treated with DMSO or Rutin for 10 weeks (N=10). Data are represented as mean ± SEM.

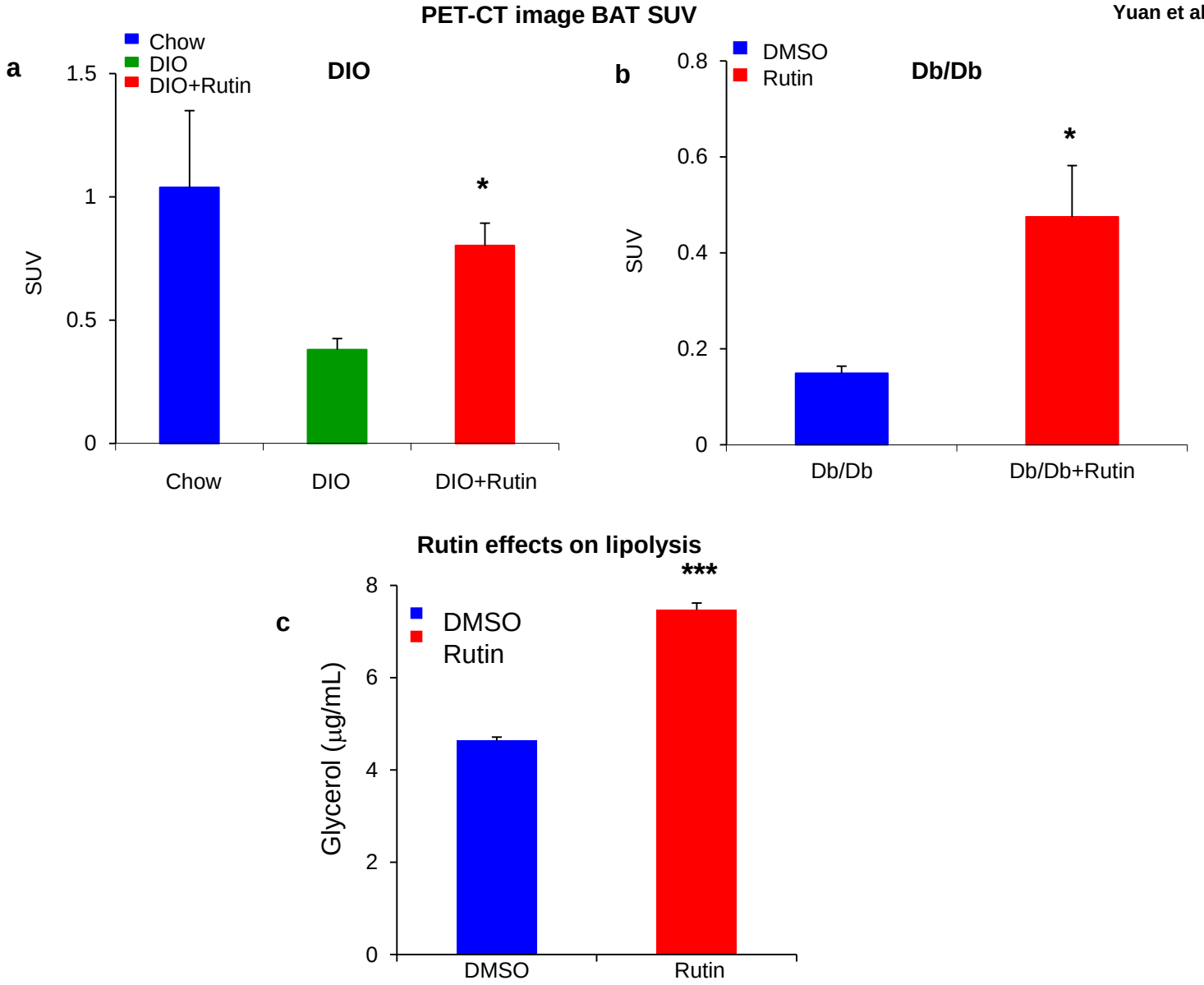

Supplementary Fig.5 PET-CT image and lipolysis assay during BAT differentiation in vitro.

a-b) The activity of brown adipose tissue in gram times the mean standard uptake value (SUV) of DIO mice (a) and Db/Db mice (b) treated with DMSO or Rutin for 10 weeks (N=10). c) Rutin treatment significant increase in vitro lipolysis during BAT differentiation (N=3-6). Data are represented as mean ± SEM. ***: $P < 0.001$, *: $P < 0.05$ versus control.